# Microscopy and spectroscopy on model catalysts in gas environments

Wenzel, S.

# Chapter 5

# Spectroscopy of Co(0001) during Fischer-Tropsch Synthesis

## 5.1 Introduction

The urgent need for sustainable means of transportation is obvious and reflected in increasingly strict regulations [204]. For certain applications such as in aviation and maritime shipping, the use of electrical motors will not be feasible in the near future. Here a sustainable solution, which does not require new infrastructure and vehicles, is the use of synthetic Fischer-Tropsch fuels. During Fischer-Tropsch synthesis (FTS) syngas, a mixture of $H_2$ and CO, is converted into long-chain hydrocarbons [205]. The syngas can stem from natural gas, oil, or renewable feedstocks such as biomass. Additionally, there is a strong research effort [206,207] to enable capture and conversion of $CO_2$ for the production of syngas, thereby closing the carbon cycle. The synthetic production of fuels cannot only reduce $CO_2$ emissions compared to conventional fuels, but the resulting fuel is cleaner as well, leading to less CO, $NO_x$, $SO_x$, and particulate matter emission than conventional diesel [208,209].
Fischer-Tropsch catalysis on a large industrial scale has been demonstrated [210,211]. Typical conditions for so-called low-temperature FTS are 30 bar gas pressure and 200 °C to 240 °C catalyst temperature [212]. Compared to iron-based catalysts, cobalt supported on various oxide supports shows higher activity and selectivity to linear alkanes [213–215]. However, cobalt catalysts are prone to multiple deactivation mechanisms, which are being researched intensively [216,217]. Among these are carbon deposition [218,219], sulfur deposition [220,221], and the oxidation of the cobalt [222–225]. Whereas there seems to be a consensus in this literature that cobalt oxide is not active, the ability of cobalt to oxidize under Fischer-Tropsch conditions has been doubted.
As oxidation states are highly sensitive to gas pressure and composition, in situ spectroscopy studies are indispensable. The use of near-ambient pressure X-ray photoelectron spectroscopy for the study of late transition metal catalysts has been reviewed recently [66]. Wu et al. [226] have used this technique to determine that, at pressures on the order of 0.1 mbar, CO reduces an oxidized cobalt foil at lower temperatures than hydrogen. In a reaction mixture of 1 CO + 1 $H_2$ the surface stayed metallic at temperatures above 225 °C suggesting that an oxidation of the foil by (background or product) water does not take place under these conditions. Additionally, they have observed carbide formation from CO at temperatures as low as 57 °C. However, it has been shown that the oxidation behavior of cobalt can depend significantly on the crystallinity, structure, and support of the cobalt sample used [227,228]. This suggests that studies on single crystals are a small but relevant contribution to completely understanding the oxidation behavior of cobalt. Kizilkaya et al. [229] find that $H_2$ more readily removes oxygen from Co(0001) than CO. Although this suggests the opposite behavior of Co(0001) compared to Co foil [226], the significantly different pressure

regime of $10^{-5}$ mbar used in Ref. [229] compared to the mbar range used in Ref. [226] could be responsible as well.
Combining the use of a single crystal with higher gas pressures, we performed near-ambient pressure X-ray photoelectron spectroscopy on a Co(0001) model catalyst. In the following we report on the cleanliness of the as-prepared crystal in UHV (Section 5.3.1), investigate the role of background water for the oxidation of Co(0001) in 0.25 mbar $H_2$ (Section 5.3.2), and compare this to the behavior in 0.25 mbar CO (Section 5.3.3). Using a theoretical model to convert measured intensities to coverages on the Co(0001) surface, we quantify the amount of surface area covered by adsorbed oxygen, different carbon species, and sulfur in $H_2$ (Section 5.3.4), CO (Section 5.3.5), and reaction conditions with a $H_2$-to-CO-ratio of 2:1 and 4:1 (Section 5.3.6).

## 5.2 Materials and Methods

### 5.2.1 Setup and Sample Preparation

The measurements presented in this chapter were performed at beamline 9.3.2 [230] of the Advanced Light Source, Berkeley and at the HIPPIE beamline [231] of Max IV Laboratory, Lund. The higher flux available at MaxIV allowed for resolving a larger number of carbon and oxygen species as exemplified in the following section. Whereas the gas exposure at ALS was realized by filling a vacuum chamber via one leak valve for each gas, the HIPPIE beamline at MaxIV uses a high-pressure cell (similar to the one described in Ref. [232]), allowing for more precise setting of flows and pressures as well as faster changes in gas composition. At the ALS we used hydrogen of purity 6.0 and CO of purity 3.0 whereas $H_2$ 4.7 and CO 3.7 were available at MaxIV. A liquid nitrogen trap was used on the hydrogen line for most of the measurements presented here. Independent of the use of the trap, the water content was below the detection limit of QMS measurements performed at MaxIV. The effects of the different gas purities and the trap are investigated in Section 5.3.2. Table 5.1 shows the water and oxygen background expected in the different bottles.

Table 5.1: Expected level of contaminants in the different gas bottles that were used [233–236]. As the values for $H_2$ 4.7 could not be found, they are estimated as the values for $H_2$ 5.0.

| Gas | Purity | Supplier | $H_2O$ Content [ppm] | $O_2$ Content [ppm] |
|---|---|---|---|---|
| $H_2$ | 6.0 | Praxair | $\leq 0.5$ | $\leq 0.1$ |
| $H_2$ | 4.7 | Air Liquide | $\leq 3$ | $\leq 2$ |
| CO | 3.0 | Praxair | $\leq 10$ | $\leq 10$ |
| CO | 3.7 | Air Liquide | $< 5$ | $< 10$ |

The Co(0001) single crystals were purchased from SPL. They were prepared by cycles of argon ion sputtering with 1 kV acceleration voltage and subsequent annealing to 590 K in UHV. The annealing temperature is limited by the phase transition from an hcp to an fcc crystal structure [237]. To additionally prevent contaminants in the bulk from reaching the surface the annealing temperature is 5 K to 10 K lower in the last cleaning cycle and the sample is kept at maximally 573 K or 300 °C during all experiments.

### 5.2.2 Resolved Species and Peak Fitting

The binding energy axis of the oxygen, carbon, and sulfur spectra was calibrated according to the metallic Co $3p_{3/2}$ peak at 59.3 eV [238] measured after every change of the photon energy. After applying this calibration, detected peaks which deviate less than ± 0.1 eV between different measurement conditions are identified as being the same species. All peak fits are done in CasaXPS 2.3.19 [239] using a Shirley background. The Co 3p peak is fitted using a metallic peak consisting of an asymmetric main peak of the shape LA(1.1,1.5,3) as well as a plasmon loss peak of shape GL(30) fixed at + 3 eV and 12.2 % peak area with respect to the main peak. Both these peaks were used for the $3p_{3/2}$ as well as the $3p_{1/2}$ part of the doublet with a fixed doublet splitting of 1.2 eV. Due to limited literature on Co 3p peak positions and fitting [238,240], this method is based on the fitting of the Co 2p peak as described below and was adjusted until a satisfactory fit for the metallic surface was found. However, for all measurement sets where the Co 3p peak was used this shape was sufficient for a satisfactory fit such that no cobalt oxide contribution needs to be considered here and only the total area underneath the metallic Co 3p doublet is relevant for the further analysis. The Co 2p peak was fitted with a main metallic peak at 778 eV of asymmetric shape LA(1,2.25,3) and two plasmon loss peaks of shape GL(30) fixed at + 3 eV and + 5 eV and 6.4 % and 2.1 % peak area with respect to the main peak, respectively. This is based on the Co 2p fitting presented in Refs. [226,241] and adjusted until a satisfactory fit for a measurement on metallic cobalt is reached. Additionally, four oxidized peaks of shape GL(40) at positions + 1.8 eV, + 4.1 eV, + 7.8 eV, and + 10 eV with respect to the metallic main peak are necessary for some measurements (see Section 5.3.2). As both CoO and $Co_3O_4$ cause a number of Co 2p contributions in the same binding energy region [241], an exact identification is complex. However, CoO has been identified on Co(0001) using in situ SXRD [242] under similar conditions as used here, which is thus the more likely candidate. Figure 5.1 shows an example fit where both metallic and oxidized cobalt are present.

For the O 1s measurements taken at the ALS, we identified oxygen peaks at 529.7 eV as adsorbed atomic oxygen O(ad), 530.8 eV as adsorbed hydroxyls OH(ad), and 532.1 eV

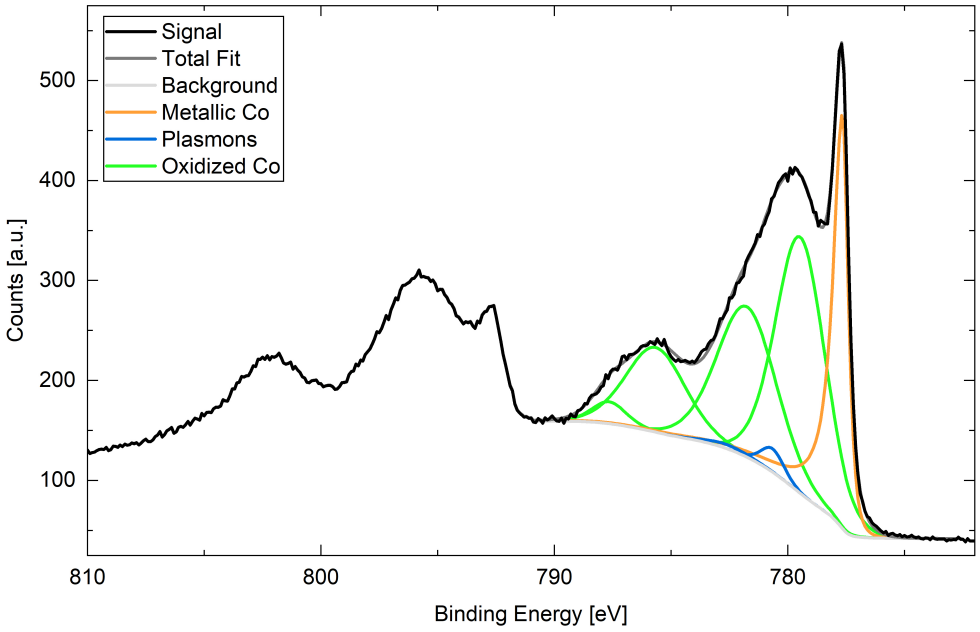


Figure 5.1: Co 2p area measured on Co(0001) in 0.25 mbar $H_2$ at 220 °C surface temperature showing all peaks necessary for a satisfactory fit of the 3/2 part of the doublet. This surface is partially oxidized, which was likely caused by a temporary technical problem with the liquid nitrogen trap that was used on the hydrogen line. For details about the oxidation behavior of Co(0001) in $H_2$ see Section 5.3.2.

as adsorbed carbon monoxide CO(ad) by comparison with relative positions given in literature [226,241,243]. These are fitted with line shapes of GL(50) and GL(70) (only adsorbed CO) and fixed binding energy distances. In the same manner [226,243] we identify carbon peaks as carbide or carbon atoms C at 283.5 eV, hydrocarbons $C_xH_y$ at 284.9 eV, and adsorbed carbon monoxide CO(ad) at 286.0 eV in the C 1s peak. The hydrocarbon contribution shifts to 285.6 eV only in UHV, which might indicate that a different type of hydrocarbon is predominantly present here compared to reaction conditions.

In the measurements done at MaxIV a larger number of species can be resolved in the C 1s peaks. An example fit with all necessary peaks is shown in Figure 5.2. The adsorbed CO is split up into four contributions: Two peaks at + 2.69 eV and + 1.50 eV with respect to the main CO(ad) peak can be identified as adsorbed CO in the presence of adsorbed atomic oxygen as they appear in agreement with the appearance of O(ad) in the O 1s signal. The main CO(ad) peak at 286.0 eV is best fitted with a slightly asymmetric LA(1.8,2.5,0) shape. Additionally, a small contribution at − 0.65 eV from the

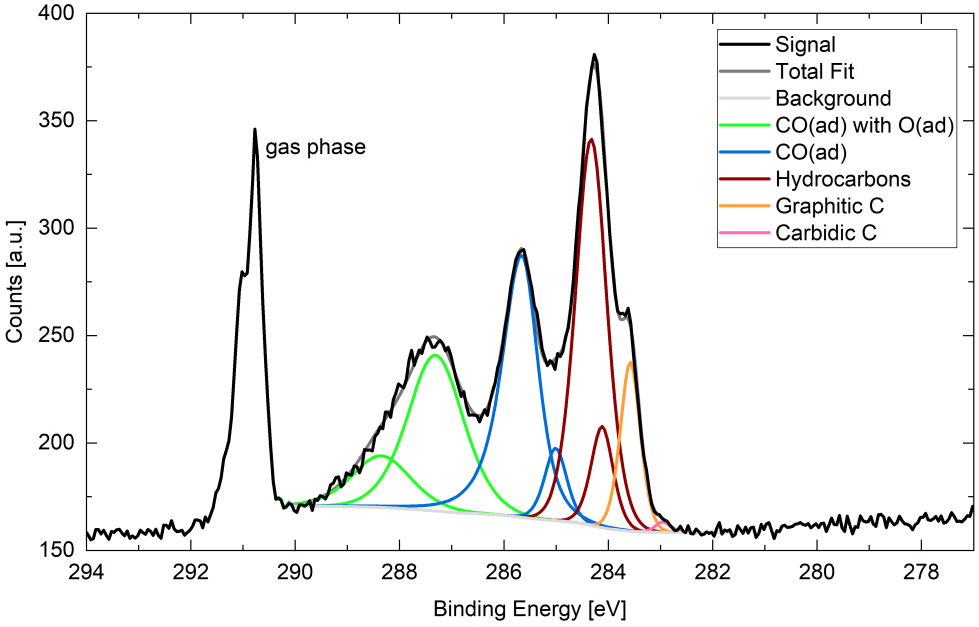


Figure 5.2: C 1s area measured on Co(0001) in 0.25 mbar CO at 190 °C surface temperature showing all peaks necessary for a satisfactory fit.

main CO(ad) peak could stem from a different adsorption site on the surface [244,245] compared to the main CO peak, but cannot be unambiguously identified on the basis of current literature or our measurements. The hydrocarbon peak is split up into two contributions at a distance of 0.2 eV from each other. It is likely that a number of different hydrocarbons are present, such that these two different peaks are necessary for a satisfactory fit. In comparison with literature [246–248] the carbide/atomic carbon contribution is split into a graphitic carbon/multiple carbon atom contribution at 283.9 eV and a carbidic/single carbon atom contribution at − 0.37 eV with respect to the first. All C 1s peaks (except the main CO(ad) peak) were fitted satisfactorily with a GL(50) shape. The relative binding energy positions of all contributions are fixed and the FWHM is restricted to the same value for every measurement of the same peak for consistency.

As in the C 1s peak, the adsorbed CO contribution to the O 1s peak is split into two parts (with and without co-adsorbed O, respectively) with a binding energy difference of 0.65 eV to each other. This can be seen in the example fits in Figure 5.3 where (a) some or (b) all of the adsorbed carbon is influenced by the adsorbed oxygen. In some conditions one additional small contribution to the O 1s signal is detected at − 1.7 eV with respect to the O(ad) contribution. It might stem from a different O

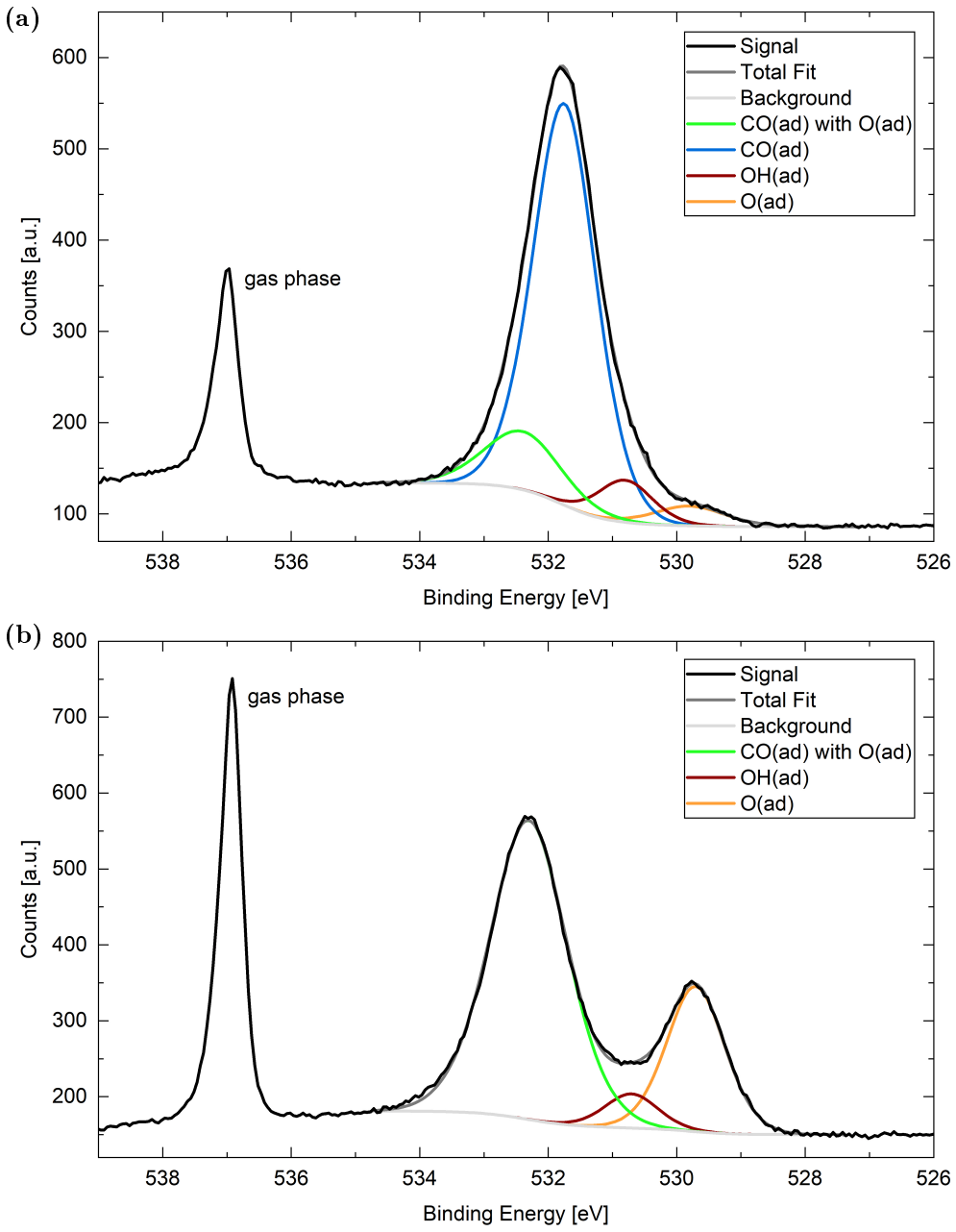


Figure 5.3: O 1s area measured on Co(0001) in 0.25 mbar CO at (a) 220 °C or (b) at 120 °C surface temperature showing the peaks necessary for a satisfactory fit.

adsorption site or a co-adsorbate, but cannot be unambiguously identified on the basis of current literature and our measurements. The area underneath this peak is therefore added to the adsorbed oxygen peak area. The adsorbed CO contribution in the O 1s signal can overlay with a contribution caused by molecularly adsorbed $H_2O$. As the exact binding energy position of the adsorbed water might vary significantly depending on co-adsorbates, the oxidation state of the cobalt, and the amount of water [226,241,249], the CO and the $H_2O$ contribution cannot be easily distinguished during peak fitting. However, on clean Co(0001) as well as on O(ad)/Co(0001) in UHV at all investigated temperatures, it can be expected that water, if it adsorbs, adsorbs dissociatively [249,250]. Therefore, the CO contribution in the O 1s signal of sets of measurements taken in UHV can be clearly identified without overlay with any signal stemming from molecular water. By comparing this CO contribution in the O 1s signal to the CO contribution in the C 1s signal from the same set of measurements we thus have a measure to evaluate whether molecular water is present on the surface. In most conditions investigated here, the ratio of the two different CO contributions is comparable to the ratio in UHV such that no molecularly adsorbed water needs to be taken into account during the analysis. One exception are measurements on an oxidized Co(0001) surface presented in Sections 5.3.2 and 5.3.4.
As no different sulfur species are resolved, the area under the S 2p peak can be determined from only the background subtraction in CasaXPS without a detailed fit. Last, when potassium was detectable, the K 2p peak partially overlapped with a second harmonic peak of the Co $2p_{3/2}$ such that a proper fit of both at the same time was necessary to determine the area underneath the K 2p doublet. GL(20) shapes with a doublet splitting of + 2.7 eV were then used for the K 2p contribution.

### 5.2.3 Converting Peak Areas to Coverages

#### Model

To convert the measured peak ares into surface coverages of all adsorbates, a mathematical description of the measured intensities is needed. In the straight line approximation [251], which only takes inelastic scattering of electrons into account, we first describe a homogeneous sample of a material $i$. In this case the amount of photoelectrons produced by a specific orbital of species $i$ in a depth $\delta$ and detected outside the surface is

$$I_i(\delta) = \phi\sigma_i W_i N_i P \cdot e^{-\delta/\lambda_i} \equiv k_i \cdot e^{-\delta/\lambda_i} \tag{5.1}$$

with the photon flux $\phi(E_p)$ at photon energy $E_p$, the cross section $\sigma_i(E_p)$ and asymmetry parameter $W_i$ of the probed orbital of species $i$ for the same photon energy, the number of atoms of species $i$ per volume $N_i$, the spectrometer efficiency $P(E_{kin})$ for

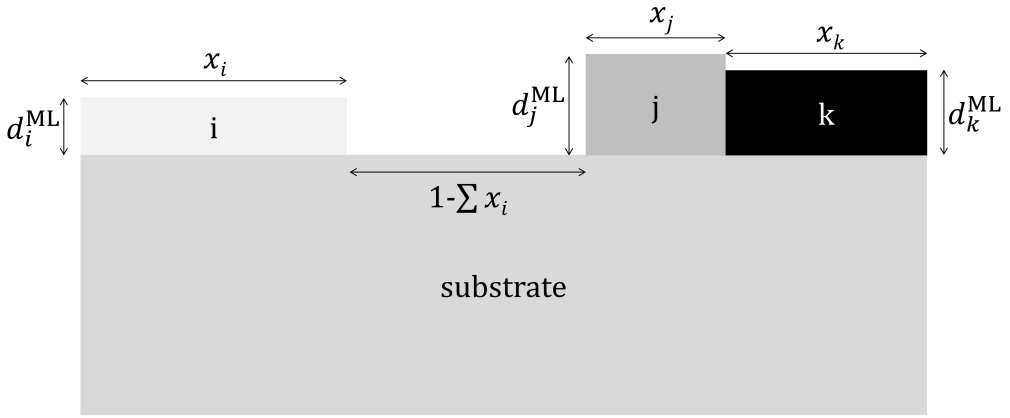


Figure 5.4: Illustration of the model assumed for coverage calculations. Explanation see text.

detection of electrons with the kinetic energy $E_{kin}$, and the inelastic mean free path $\lambda_i(E_{kin})$ of the same electrons in material $i$.
Integrating Equation 5.1 over a homogeneous, clean, and macroscopically thick ($\delta \to \infty$) cobalt substrate results in the total contribution from the specific orbital and thus the area under the measured peak of

$$I_{\mathrm{Co}}^{\mathrm{sub}} = k_{\mathrm{Co}}\lambda_{\mathrm{Co}}. \tag{5.2}$$

Figure 5.4 illustrates how this is extended to include different adsorbed species. For an adsorbate $i$ covering an area $x_i$, with $0 \leq x_i \leq 1$, Equation 5.1 has to be integrated over the thickness of the first monolayer $d_i^{\mathrm{ML}}$ resulting in

$$I_i^{\mathrm{ad}} = x_i \cdot k_i\lambda_i \left(1 - e^{-d_i^{\mathrm{ML}}/\lambda_i}\right). \tag{5.3}$$

For a part of the cobalt substrate which is covered with an adsorbate $i$ the substrate intensity given in Equation 5.2 is attenuated due to the adsorbate by a factor of $e^{-d_i^{\mathrm{ML}}/\lambda_i}$. On the other hand, the area $1-\sum_i x_i$ of the cobalt follows Equation 5.2 without attenuation. Notice that this is only valid if all possible adsorbates $i$ are taken into account. The total cobalt signal is then

$$I_{\mathrm{Co}} = k_{\mathrm{Co}}\lambda_{\mathrm{Co}} \cdot \left(\left(1 - \sum_i x_i\right) + \sum_i x_i \cdot e^{-d_i^{\mathrm{ML}}/\lambda_i}\right) \tag{5.4}$$

$$= k_{\mathrm{Co}}\lambda_{\mathrm{Co}} \cdot \left(1 - x_j \sum_i (x_i/x_j) \cdot \left(1 - e^{-d_i^{\mathrm{ML}}/\lambda_i}\right)\right) \tag{5.5}$$

where the second notation is simply for the purpose of convenience for the following steps. With the above equations we can express the ratio of intensities of two different

adsorbates $I_i/I_j$ as well as the ratio of the intensity of an adsorbate and the cobalt substrate $I_i/I_{\mathrm{Co}}$ and subsequently solve for the following equations.

$$\frac{x_i}{x_j} = \frac{I_i}{I_j}\frac{k_j\lambda_j}{k_i\lambda_i}\frac{\left(1-e^{-d_j^{\mathrm{ML}}/\lambda_j}\right)}{\left(1-e^{-d_i^{\mathrm{ML}}/\lambda_i}\right)} \tag{5.6}$$

$$x_j = \left(\frac{I_{\mathrm{Co}}}{I_j}\frac{k_j\lambda_j}{k_{\mathrm{Co}}\lambda_{\mathrm{Co}}}\left(1-e^{-d_j^{\mathrm{ML}}/\lambda_j}\right) + \sum_i (x_i/x_j)\cdot\left(1-e^{-d_i^{\mathrm{ML}}/\lambda_i}\right)\right)^{-1} \tag{5.7}$$

We have found it most convenient to first calculate $x_i/x_j$ for all $x_i$ and one specific adsorbate $j$ using Equation 5.6, then calculating the $x_j$ from $I_{\mathrm{Co}}/I_j$ and all $(x_i/x_j)$ using Equation 5.7, and finally getting all other $x_i$ as $x_i = (x_i/x_j)\cdot x_j$.

**Multiple Layers**

One complication in applying this model in our scientific case is that over time the overlayer of one of the adsorbed materials, the hydrocarbons, can become thicker than one monolayer under specific conditions (see Section 5.5.1). This introduces another unknown, the height of that hydrocarbon overlayer. To take this into account the sum of all coverages $\sum_i x_i$ is monitored. Once the result would be larger than 1 the equations as above do not hold anymore and the calculation needs to be adjusted slightly. For this the coverage of an adsorbate for which the measured intensity does not significantly change over time (anymore) in these conditions, we used oxygen or sulfur, is fixed to the last calculated value. All other coverages are calculated as above and the coverage $x_{\mathrm{hc}}$ of the hydrocarbons is then $1-\sum_{i\neq\mathrm{hc}} x_i$. Now the ratio of the oxygen or sulfur and the hydrocarbon intensities can be used to calculate the height $D_{\mathrm{hc}}$ and thus number of monolayers of the hydrocarbons as

$$D_{\mathrm{hc}}/d_{\mathrm{hc}}^{\mathrm{ML}}. \tag{5.8}$$

We finally plot the corresponding number of monolayers that were present if it were the only adsorbate on the surface $X_{\mathrm{hc}} \equiv x_{\mathrm{hc}}\cdot D_{\mathrm{hc}}/d_{\mathrm{hc}}^{\mathrm{ML}}$. As this procedure assumes that all of the hydrocarbons are layered to the same height $D_{\mathrm{hc}}$ on only one specific fraction $x_{\mathrm{hc}}$ of the substrate surface area, this model is limited and can easily become inaccurate, especially for large coverages. The manner in which the hydrocarbons grow, layer-by-layer or three-dimensional growth as well as potentially on top of other adsorbates, is unknown and neglected here.

In the case of the oxidation in $H_2$ at temperatures below 220 °C (see Section 5.3.2) the model results in (oxygen) coverage values large than 1 as well. As here not only the adsorbate O(ad) is present in multiple layers but a cobalt oxide is growing, the

model cannot be extended in a similar fashion and the situation would require a more complex model making assumptions about the fashion in which this oxide grows, which is outside the scope of this thesis. Therefore, the results of our model for this case are intentionally reported only as relative coverages of the different adsorbed species instead of absolute coverages and can only be discussed in a qualitative manner.

### Estimating Parameters

The photon flux $\phi(E_p)$ was recorded during the measurements after every change of the photon energy (ALS) or read from a pre-recorded flux curve (MaxIV). The cross sections $\sigma_i(E_p)$ of Co 2p, Co 3p, O 1s, C 1s, and S 2p for the specific photon energies were determined using Ref. [252] and are displayed in Table 5.2. The asymmetry parameters $W_i$ are equal to 1 as the setups used here adhere to the "magic angle" in XPS [64]. As only ratios of intensities measured in the same geometry and at the same electron kinetic energy are compared, the spectrometer efficiency $P(E_{kin})$ does not need to be known. The inelastic mean free path was calculated according to the TTP-2M equation with the help of the NIST Database 71 Version 2.1 [253]. For the bulk cobalt metal the mean free path can be taken directly from the database. For all adsorbates the calculation requires an estimation of the mass density $m_i$, the number of valence electrons $V$ of the material (contributing to electron loss), and a rough estimate of the bandgap $E_\mathrm{g}$ of the material. A recommendation for the choice of $V$ is given in the manual to the NIST Database [253]. For estimation of the mass density, the number of atoms per volume $N_i$, and the thickness of one monolayer $d_i^{\mathrm{ML}}$ we distinguish two different cases.

Most measurements shown in this thesis are of the first case, in which less than a monolayer of an adsorbate is expected. Then the structure likely differs significantly from any bulk structure of the adsorbate and the crystal structure of the Co(0001) substrate thus needs to be taken into account. In this case the topmost cobalt layer has to be included in the calculation of $\lambda$ and thus contributes to the mass density, the valence electrons, and the bandgap. Theory supplies values for the Co-O distance for adsorbed O and OH [254], Co-C distance for adsorbed C [255], and the Co-S distance for sulfur [256], which are used to estimate the monolayer thicknesses. Together with the cobalt crystal structure [257] these are used to calculate the mass density and number of probed atoms per volume geometrically. The rough bandgap estimations were done using literature values for cobalt oxide [258] as well as different sulfides and carbides [259]. For the case of CO, the measurement of the C 1s signal as well as the O 1s signal are available to include into the model. Based on theory literature [260] we assume an upright adsorption with the carbon atoms towards the surface and use the Co-C as well as the C-O distance for the layer thicknesses. These are used separately

Table 5.2: Estimated parameters for the calculation of coverages. Explanation and sources see text.

| Species | Peak | $E_p$ [eV] | $\sigma$ [Mbarn] | $d^{\mathrm{ML}}$ [nm] | $N$ $[(\mathrm{nm})^{-3}]$ | $m$ $[\mathrm{g}\cdot(\mathrm{cm})^{-3}]$ | $V$ | $E_\mathrm{g}$ [eV] | $\lambda$ [nm] |
|---|---|---|---|---|---|---|---|---|---|
| O | O 1s | 730 | 0.2551 | 0.18 | 99.8 | 5.89 | 15 | 2.5 | 0.685 |
| OH | O 1s | 730 | 0.2551 | 0.20 | 92.5 | 5.75 | 16 | 2.5 | 0.697 |
| CO | O 1s | 730 | 0.2551 | 0.12 | 152.7 | 5.27 | 19 | 3 | 0.709 |
| CO | C 1s | 480 | 0.2987 | 0.18 | 103.0 | 5.27 | 19 | 3 | 0.709 |
| C | C 1s | 480 | 0.2987 | 0.21 | 87.3 | 5.2 | 13 | 3 | 0.299 |
| $C_xH_y$ ($<$ 1 ML) | C 1s | 480 | 0.2987 | 0.34 | 50.4 | 1.19 | 86 | 14.5 | 2.278 |
| $C_xH_y$ (bulk) | C 1s | 480 | 0.2987 | 0.34 | 32.5 | 0.76 | 86 | 14.5 | 2.371 |
| S | S 2p | 365 | 1.2080 | 0.16 | 114.6 | 57.6 | 15 | 3 | 0.592 |
| Co | Co 3p | 260 | 0.7197 | 0.21 | 90.1 | 8.8 | 9 | | 0.544 |
| Co | Co 2p | 980 | 0.7651 | 0.21 | 90.1 | 8.8 | 9 | | 0.544 |

for the calculation of $N$ for the O 1s signal and the C 1s signal. The CO contribution in the C 1s signal is additionally calibrated to take the attenuation by the oxygen atoms on top into account. Thus, the measured intensities are divided by a factor of $\exp(-d^{\mathrm{ML}}_{(\mathrm{O\ of\ CO})}/\lambda_{\mathrm{CO}})$. However, the thickness of the whole CO molecule $d_{\mathrm{CO}} = d_{(\mathrm{C\ of\ CO})} + d_{(\mathrm{O\ of\ CO})}$ is then taken into account for the calculation of $m$ and $\lambda$ as well as the attenuation of the cobalt signal in the area covered with CO. The adsorbed hydrocarbons are a more complex case as a large number of different molecules could be present. Navarro et al. [47] investigated the Co(0001) surface using in situ scanning tunneling microscopy during FTS under similar conditions as studied here. The main product length detected on the surface was 14 carbon atoms with each molecule taking up an area of 1.8 nm by 0.46 nm and an apparent overlayer height of 0.11 nm. However, the height can be underestimated in the STM due to limited conductivity. Graphene already has a higher thickness of 0.21 nm on Co(0001) as determined by DFT [255] similar to the thickness of benzene on Co(0001) of 0.22 nm [261]. We choose a more generous estimate of 0.34 nm on the hands of the layer thickness of graphite [195]. Using the surface area taken up by one molecule and the height estimate we can again calculate $m$ and $N$.

In the second case, when significantly more than a monolayer of a certain adsorbate is expected to be present, it is likely that the structure is similar to the structure the adsorbate has when it is present in bulk. This is the case for adsorbed hydrocarbons in some measurements under the conditions described in Section 5.5.1. Then literature values for $E_{\mathrm{g}}$ [262] and $m$ [263] of $C_{14}H_{30}$ can be used to calculate the number of probed atoms per volume $N$. In this case the thickness of one monolayer is thus not needed for the calculation of $N$, but can be used in the last step of the calculation in Equation 5.8 in order to convert the resulting total overlayer thickness into a number of layers. We choose the same estimate of 0.34 nm as described for the first case above.

#### Test and Calibration

When applying this model to a series of measurements it became clear that it is not complete. A rough estimate of peak areas from a cobalt survey spectrum measured at 1130 eV photon energy shows that the order of magnitude of the Co 3p, Co 3s, and Co 4s peaks does agree with the literature values of the cross sections confirming the validity of the general approach of our model as well as the literature values. In contrast, the peak area of the Co 2p peak in the survey is at least an order of magnitude higher than expected from the cross section. This estimate was done without taking the different probing depths for the different peaks into account. As Co 2p has the highest binding energy, the probing depth is lowest such that the discrepancy should be even larger. This agrees with the discrepancy of a factor of about 50 that results

from fitting detailed Co 2p and Co 3p peaks taken at the same probing depth with an electron kinetic energy of 200 eV. This value was obtained by averaging over 20 different measurements taken on different days. From these observations the following can be excluded as causes for the discrepancy: repeated changing of slits being irreproducible, the flux curve for the different photon energies being imprecise, and the same slit setting leading to varying attenuation depending on the photon energy. It is likely that the crystalline structure of the substrate, which is not taken into account in our model at all, could have a strong influence on the production of photoelectrons and the complex loss processes in the material. Investigating this further is out of the scope of this thesis.

However, it follows that the coverage model has to be complemented by experimental calibration factors for the different peaks which are measured. First, we calibrate the ratio of the O 1s and the Co 2p (or Co 3p) signal such that the adsorbed oxygen contribution in UHV corresponds to the 0.25 monolayer coverage expected when assuming maximum coverage with the 2x2 overlayer on Co(0001) [229]. The calibration factor was determined from the cleanest as-prepared sample measured in UHV. A second as clean sample measured on a different day, resulted in a calibration factor deviating from the first by 1 %, which evidences that this calibration method is reproducible. The measurements used were done at 220 °C. But, as we will show in Section 5.3.1, the measured signal of adsorbed oxygen in UHV is not temperature dependent between 140 °C and 300 °C.

Second, the C 1s to O 1s signal ratio is calibrated such that the two different CO coverages, calculated from the carbon and the oxygen signal respectively, are in agreement. This calibration factor is an average over at least 20 different measurement sets in different gas and temperature conditions. However, as explained in Section 5.2.2, the CO contribution to the O 1s signal cannot be clearly determined from measurements where molecularly adsorbed water is present on the surface. These are therefore not taken into account for the calculation of this calibration factor. In all other gas compositions the calculated ratio of the CO contributions in C 1s and O 1s roughly agrees with the ratio in UHV. Therefore, the resulting calibration factor we have used is free from the possible influence by the contribution from molecularly adsorbed water.

Third, the coverage of species calculated from peaks for which there is no calibration measurement, S 2p in our case, should be merely seen as an estimate of the order of magnitude and used for relative comparison of the coverage in different situations or changes over time rather than as an absolute value.

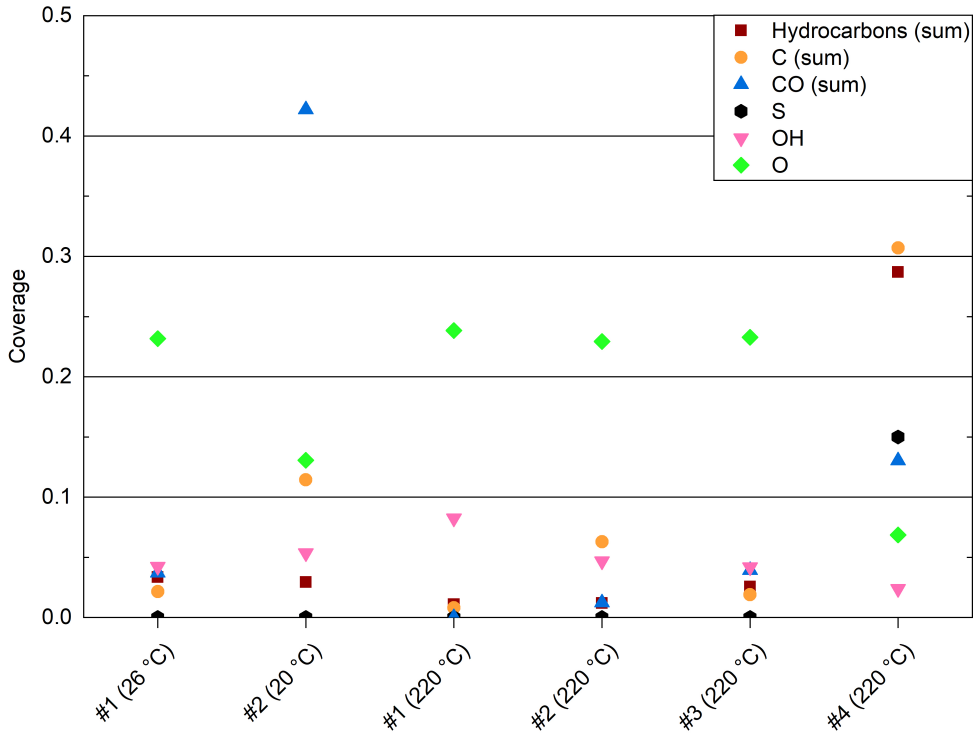


Figure 5.5: Coverages of all measured adsorbed species on four different as-prepared Co(0001) samples in UHV at roughly room temperature or 220 °C. For a better overview the different carbon, hydrocarbon, and adsorbed CO peaks are summed up to one coverage each here and are only displayed in detail in the supplemental information.

## 5.3 Results and Discussion

### 5.3.1 As-prepared Co(0001) in UHV

Figure 5.5 displays the calculated coverages comparing multiple as-prepared samples in UHV at room temperature and at 220 °C. On average the oxidized contribution in the Co 3p or Co 2p peaks measured in UHV is 3 % of the total depth of cobalt probed. The O contribution in the O 1s signal is thus mainly due to adsorbed atomic oxygen on metallic cobalt in UHV. At room temperature it is noticeable that sample # 1 has a coverage of adsorbed oxygen of 0.23, whereas sample # 2 only has 0.13. On the other hand, sample # 2 shows more adsorbed CO, 0.42 compared to 0.04 CO on sample # 1, which leaves less adsorption sites for the oxygen. As both water and CO are common background gases in UHV and known to adsorb on Co(0001) at room temperature

[245], in the case of water dissociatively forming adsorbed O [249], it is likely that the coverages can differ depending on the exact composition of the UHV background. Whereas sample # 1 was measured in a freshly baked UHV chamber, sample # 2 was measured after CO had been used in the high-pressure cell, thus in an increased CO background, although the pressure had recovered to the $10^{-9}$ mbar range. Figure 5.20(a) in the supplemental information indicates that an increased CO adsorption at the expense of adsorbed O (sample # 2 at 20 °C and sample # 4 at 220 °C) is mainly detected as an increase in the peak identified as CO without co-adsorbed O rather than the peak associated with CO co-adsorbed with O, therefore confirming the validity of the peak fitting method. However, the separation of the two peaks is not accurate enough for a quantitative comparison with the O coverage, especially at low total CO coverages.

Under heating to 220 °C most of the adsorbed CO desorbs also in the high CO background. At this temperature the CO coverage is between 0 and 0.04 on samples # 1 to # 3, whereas the O coverage remains at 0.23 to 0.24. The OH coverage, which likely stems from the $H_2O$ dissociation as well, lies between 0.04 and 0.08. Carbon and hydrocarbon contaminants cover maximally 0.06 and 0.03 of the surface, respectively, for samples # 1 to # 3. Hereby, the detailed peak fitting (see Figure 5.20(b) in the supplemental information) shows that carbon is mainly present as carbidic carbon. In most samples the carbidic peak represents at least 95 % of the summed-up C peak area in UHV with one exception (67 % carbidic C and 33 % graphitic C on sample # 3). On the other hand, the two different types of hydrocarbons do not show a clear trend in UHV as both can represent between 0 % and 100 % of the total hydrocarbons (see Figure 5.20(c) in the supplemental information).

Sample # 4 is more contaminated compared to samples # 1 to # 3. It shows 0.29 coverage with hydrocarbons and 0.31 coverage with atomic carbon. At the same time a higher coverage with CO (0.13) is possible in this state, which can either be related to the other co-adsorbates or this surface is rougher than the other samples, which would leave more low-coordinated surface atoms, steps and kinks, for the CO adsorption. The Co(0001) terraces are expected to be free from CO above roughly 130 °C in UHV [245]. Obviously, a sample like sample # 4 has to be subjected to more sputtering and annealing before performing any experiments.

No sulfur was detected on the other samples after preparation in UHV. On one as-prepared sample traces of potassium could be detected. By a rough comparison of the K 2p signal to the C 1s signal and the respective photon cross sections at 480 eV photon energy, the potassium coverage was estimated to be on the order of 0.001 at 20 °C and increasing to an order of 0.01 when heating to 300 °C. Therefore, the potassium was not included in the coverage model applied here. The temperature dependence

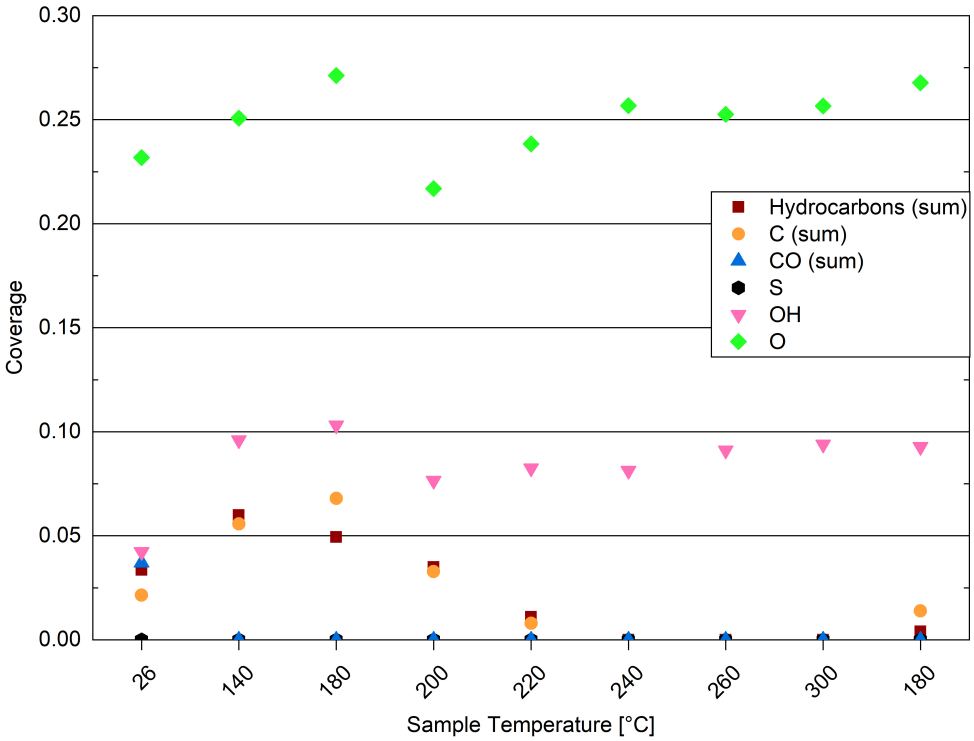


Figure 5.6: Coverages of all adsorbed species on one as-prepared sample in UHV (sample # 1) at different temperatures. Details see text.

suggests that the potassium is present in the bulk of the cobalt crystal and can reach the surface upon heating. The manufacturer excludes their starting material, as well as processing materials and tools as the source of the potassium. However, it could stem from polymer materials inside the vacuum chamber [264]. On the as-prepared samples used for the measurements in Sections 5.3.2 to 5.3.6 the potassium was below the detection limit. These were subjected to at least 100 more cleaning cycles.

Figure 5.6 shows the temperature dependence of the UHV characterization of sample # 1. In the whole probed range from room temperature to 300 °C the adsorbed oxygen remains at a coverage of $0.25 \pm 0.04$. From this we generously estimate a maximal uncertainty of $\pm 0.05$ for all calculated coverages in the following sections. The temperature stability suggests that the adsorbed oxygen might be stable under the annealing to 317 °C during the sample preparation. This is in agreement with temperature-programmed desorption experiments by Xu et al. [249], in which the adsorbed oxygen formed by water dissociation was stable until at least 350 °C. In the measurements

presented here the adsorbed OH coverage remains between 0.075 and 0.1 upon heating to 300 °C as well. A lower value of 0.04 is only measured at room temperature where more CO is present on the surface possibly blocking the adsorption sites. The CO has desorbed from 140 °C on, which is in agreement with temperature-programmed desorption reported in the literature (see Figure S1 in Ref. [245]). The surface area covered with hydrocarbons from the UHV background seems to increase upon heating to 140 °C, which might be due to outgassing of parts of the sample holder during this first heating in the analysis chamber. Upon further heating the hydrocarbons desorb and are not detectable from 240 °C on. Cooling down again to 180 °C, a coverage of 0.01 with hydrocarbons adsorbs again.
The atomic carbon coverage increases from 0.02 to 0.07 when heating to 180 °C and decreases again upon further heating until it is not detectable anymore from 240 °C on. This is somewhat surprising as the dissolution of carbon in cobalt is only expected at significantly higher temperatures where cobalt carbide can be formed [265]. Theory suggests that carbon atoms can easily diffuse below the topmost surface layer of Co(0001), whereas they are unlikely to diffuse deeper into the bulk unless Co vacancies are present [266]. Carbon atoms right below the topmost surface layer should still be detectable in our case as we probe the two to three topmost layers of the cobalt crystal. This is estimated by comparing the inelastic mean free path of 0.544 nm at 200 eV electron kinetic energy (see Section 5.2.3) to the layer thickness of Co(0001) of 0.21 nm (calculated from the crystal structure [257]). However, the existence of vacancies is likely on a Co(0001) surface, especially as the annealing temperature is limited, such that the dissolution to lower layers cannot be excluded as an explanation for not detecting the carbon at these temperatures. Cooling down to 180 °C a carbon coverage of 0.01 resurfaces, which is an order of magnitude less than the 0.14 that was present at 140 °C before heating up. In general, it is clear that keeping the surface at an elevated temperature (between 220 °C and 260 °C) in UHV and when introducing gases can increase the surface cleanliness and keep the surface free from CO, carbon, and hydrocarbons.

### 5.3.2 Oxidation of Co(0001) in Hydrogen

Figure 5.7 compares the change in the O 1s signal measured at MaxIV while introducing (a) wet and (b) dried hydrogen, respectively, both at 220 °C surface temperature. Both samples show some adsorbed oxygen when starting from UHV as discussed in detail in the previous section. When introducing the wet hydrogen, the oxygen signal strongly increases, whereas the dried hydrogen removes the adsorbed oxygen from the as-prepared sample. The horizontal reference lines in Figure 5.7(b) show that the adsorbed oxygen can already be removed before actually starting the flow of 3.8 ml/min

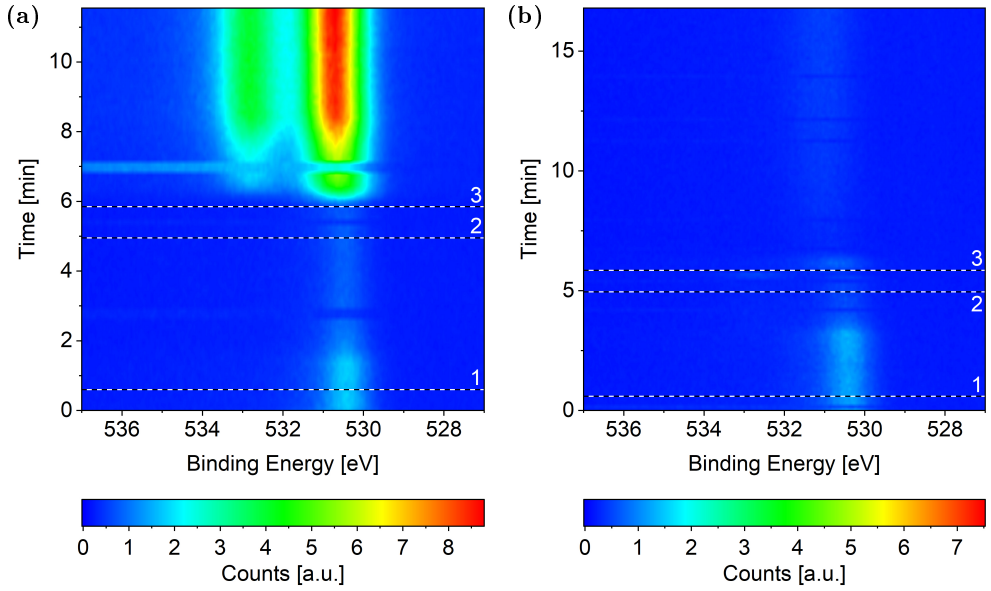


Figure 5.7: O 1s area measured on Co(0001) over time while introducing (a) wet and (b) dried $H_2$, respectively, both at 220 °C. The black and white reference lines mark (1) the closing of the near-ambient pressure cell, (2) the enabling of the mass flow controller, (3) and the start of the flow of $H_2$ (details see text). All scans in each map were normalized to have the same background level. In (a) two consecutive scans at around 7 min as well as around 3 min do not agree with the scans before and after. Such faulty scans can be caused by mechanical movements on the machine, for example when closing the cell door, or when the detector does not move to the correct energy range in time (meaning that the delay time between different peaks is not chosen long enough). In (b) such faulty scans might be present at 0 min and around 6 min.

$H_2$ (at the time of reference line 3). When closing the cell door (at reference line 1) the volume is not pumped via the analysis chamber anymore such that the composition of the vacuum background can change. Subsequently, the gas lines are opened to the cell (no reference line) such that the background composition can be influenced by the background in the gas lines as well. Additionally, when the mass flow controller is enabled (at reference line 2), meaning a valve between the mass flow controller and the gas lines to the cell is opened, some gas could easily enter the cell as mass flow controllers might not be completely leak-tight when closed. These complications in knowing the exact gas composition at every point in time could also explain why it appears that the adsorbed oxygen on the as-prepared sample is (partially) removed in Figure 5.7(a) before it strongly increases in the flow of wet $H_2$.

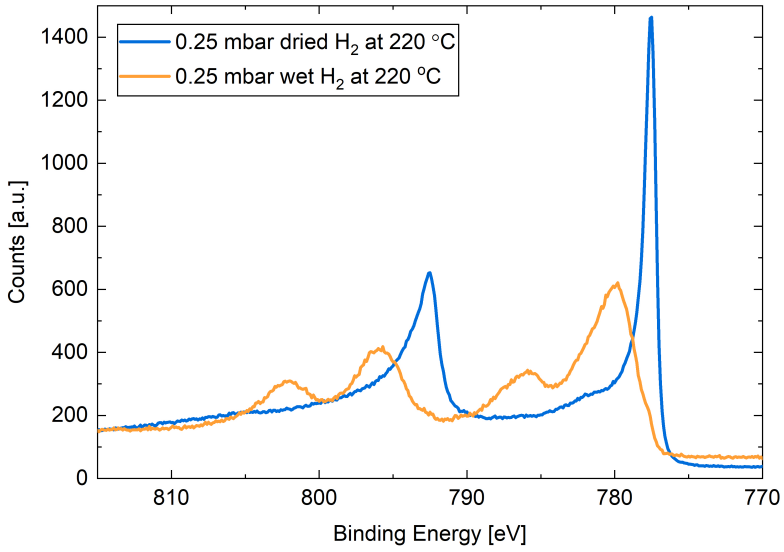


Figure 5.8: Co 2p area measured on Co(0001) after roughly 30 min in 0.25 mbar dried $H_2$ (blue) compared to after roughly 10 min in wet $H_2$ (orange), both introduced at 220 °C. The latter spectrum was only measured shortly after CO was added to the gas composition. However, as will be shown in Section 5.3.3, the presence of CO does not oxidize the cobalt surface, such that this measurement can still be used to estimate the extent of oxidation caused by wet $H_2$.

Apart from the adsorbed oxygen or oxide signal at 530.4 eV, a second contribution is visible in Figure 5.7(a). The binding energy is roughly the one we have identified as the binding energy of CO co-adsorbed with O. However, in this case there is no measurable carbon signal at the time of the last spectrum of the map, such that the same peak needs to be identified as molecularly adsorbed water (see Section 5.2.2). If the water dissociates, the binding energy of the resulting adsorbed OH would lie between the adsorbed O or oxide and the adsorbed $H_2O$, such that it might not be clearly resolved as a distinct peak in Figure 5.7(a). A detailed fit of the last spectrum in the map results in 29 % of the oxygen signal stemming from adsorbed water and merely 2 % from adsorbed OH. Thus, the water is mainly adsorbed molecularly in this case. As shown in the following paragraph, the cobalt is oxidized here, which explains why it is inactive for water dissociation [249].
The Co 2p peaks displayed in Figure 5.8 suggest that the probed depth of the cobalt sample is almost completely oxidized by the wet hydrogen. 98 % of the peak area in a detailed fit is the oxidized contribution. The strong contribution in the O 1s signal can thus be identified as mainly stemming from cobalt oxide instead of adsorbed atomic

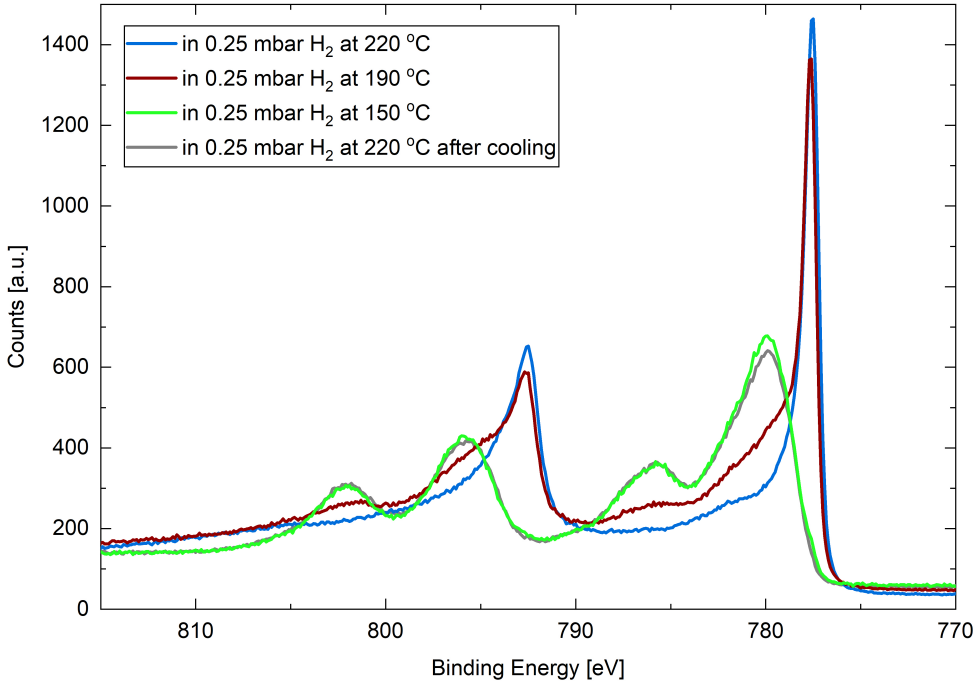


Figure 5.9: Co 2p areas measured on Co(0001) in 0.25 mbar dried $H_2$ at 220 °C, 190 °C, and 150 °C, as well as after subsequent heating to 220 °C.

oxygen in this case. In comparison, the surface stays mostly metallic in the dried hydrogen. The detailed fit shows 9 % oxidized contribution in the Co 2p peaks, which is not more than the maximum measured on an as-prepared sample in UHV.

While the dried hydrogen keeps the cobalt surface metallic in 0.25 mbar at 220 °C, it does oxidize upon reduction of the temperature. Figure 5.9 shows the Co 2p area in 0.25 mbar dried $H_2$ under cooling down from 220 °C to 190 °C and 150 °C, as well as under subsequently increasing the temperature to 220 °C again. The sample was kept at every temperature for about 1 h. Within this time frame a partial oxidation at 190 °C is clearly visible in the Co 2p area (red curve). A detailed fit identifies 38 % of the probed depth measured as oxidized cobalt. While staying in these conditions, the O 1s area was measured twice with a time difference of 26 min, over which no change is measurable (data not shown). Thus, the full oxidation measured at 150 °C another 29 min later (green curve) is likely actually caused by this decreased temperature and would have not taken place at 190 °C, at least not within this time frame.

Figure 5.9 additionally displays the Co 2p area after increasing the temperature of the oxidized surface from 150 °C to 220 °C (grey curve), where it is not reduced within

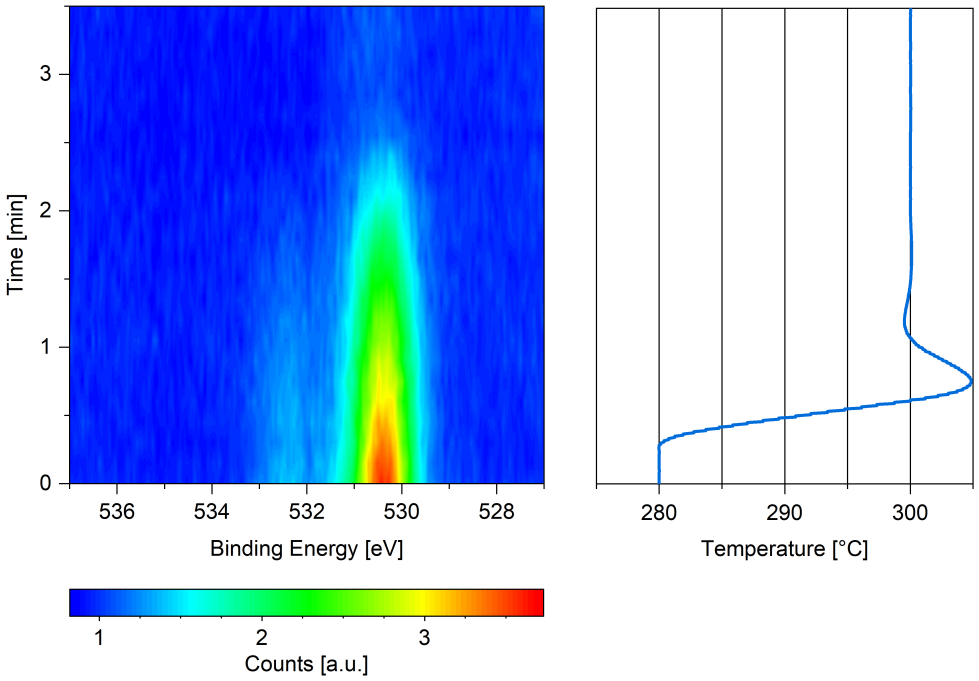


Figure 5.10: O 1s area measured on previously oxidized Co(0001) in 0.25 mbar dried $H_2$ while increasing the temperature from 280 °C to 300 °C with the corresponding temperature graph.

1 h and two measurements of the O 1s area with a time difference of 36 min do not show any change. This suggests that the reduction is kinetically limited in the time frame investigated here. Upon further increasing of the temperature the sample is reduced within 2 min above 280 °C. This is evidenced by the change of the O 1s signal displayed next to the sample temperature in Figure 5.10. A 90 % metallic contribution was subsequently measured in the Co 2p area at 300 °C. However, the increase of the temperature from 220 °C to 280 °C, over which no significant change in the O 1s area was visible, took place within only 15 min, leaving the possibility that a lower temperature might have been sufficient for reduction over the course of hours.
In measurements taken at the ALS in purer $H_2$ (see Table 5.1) as well as using a liquid nitrogen trap the cobalt stayed completely metallic at 180 °C (data not shown). However, lower temperatures were not tested in this case and a possible disagreement between the temperature read-out in the two different systems is not unlikely. This can be caused by different positioning of thermocouples with respect to the sample, different thicknesses of the thermocouples, as well as different distances between the sample and other materials picking up the thermocouple signal. Therefore, this is no

clear evidence that the initial purity of the gas in the bottle has an influence. However, the difference between wet and dried hydrogen used at MaxIV is clearly evidencing at least some influence of the water background on the oxidation behavior in hydrogen. As hydrogen adsorbed on the terraces of Co(0001) is more stable than on the steps and defects [267,268], these lower-coordinated Co sites could be free for dissociative $H_2O$ adsorption as soon as the temperature is low enough in the specific $H_2O$ partial pressure. DFT calculations by Ma et al. [269] suggest that the adsorption of $H_2O$ is significantly easier on the steps than on the terraces, whereas the dissociation is only slightly enhanced in comparison. Once some $H_2O$ has dissociated, the resulting adsorbed O can strongly promote further $H_2O$ dissociation on the terrace [249,270] and even more so on the steps [269]. The oxidized CoO/Co(0001) terraces are not active for further water dissociation [249], such that a limited growth of only one layer of oxide could be expected. However, to our knowledge there are no similar studies regarding the water dissociation on the steps and defects of oxidized cobalt. As the measurements presented here probe between two and three layers of the single crystal, which appear fully oxidized, we cannot directly confirm or exclude a limited growth. Under vacuum pressures, where hydrogen has been shown to remove adsorbed oxygen from Co(0001) from roughly 180 °C on [229] and no oxidation caused by $H_2$ has been reported, the background water pressure could be significantly lower leading to less water adsorption and dissociation. The same study finds that a higher temperature is needed for $H_2$ to remove adsorbed oxygen from defective Co(0001) compared to the Co(0001) terraces, which confirms that it is less effective at the low-coordinated sites. The oxidation observed here in the mbar range has been observed previously by Groot et al. [242] in ambient-pressure surface X-ray diffraction on Co(0001) showing the formation of crystalline CoO in 1 bar $H_2$ when decreasing the temperature from 220 °C to 180 °C. Interestingly, although these studies were done without any drying of the gas (purity of the hydrogen between 4.5 and 5), the surface stayed metallic at 220 °C and reduced again when increasing the temperature to 220 °C after the oxidation. These observations indicate a more efficient reduction in 1 bar wet $H_2$ compared to 0.25 mbar dried $H_2$. The difference in total pressure might lead to a larger hydrogen coverage at the same temperature, thus more efficiently preventing the adsorption and dissociation of water and removing the oxygen atoms. Especially, the reduction when returning to 220 °C indicates that it is less kinetically limited at higher pressure compared to our measurements. In a pressure of 0.2 mbar $H_2$, Papaefthimiou et al. [228] have reduced an oxidized Co(0001) surface at about 250 °C, which is the same range as our result taking the usual inaccuracies of temperature measurements into account. Additionally, our measurements agree with the results of Wu et al. [226] on polycrystalline cobalt foil. In roughly 0.13 mbar (100 mTorr) $H_2$ they observe

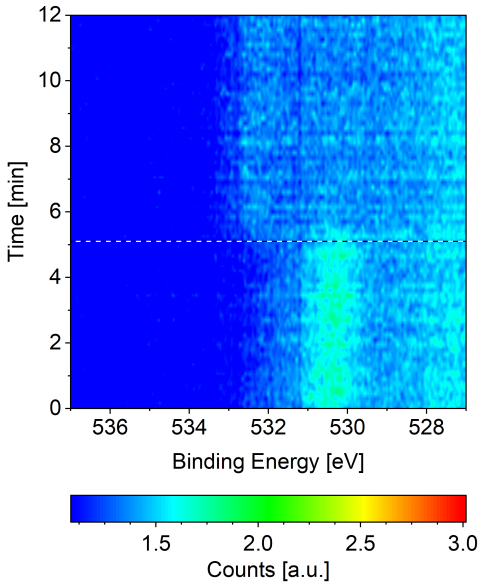


Figure 5.11: O 1s area measured on Co(0001) over time while introducing CO at 220 °C. The black and white reference line marks the start of the flow of 1.9 ml/min CO.

oxidation below 185 °C and the reduction between 200 °C and 290 °C indicating that the difference in structure between the single-crystalline and the polycrystalline sample might not have a significant influence on the oxidation behavior in this pressure range of hydrogen. Lukashuk et al. [271] have observed the reduction of a $Co_3O_4$ powder in 0.4 mbar $H_2$ starting from 250 °C on as well. In contrast, Turczyniak et al. [227] observe a complete reduction of $Co_3O_4$ nanopowder in 0.2 mbar $H_2$ only at 350 °C. This confirms that the complex structure of nanoparticles and powders, which can consist of numerous different types of cobalt sites, not even taking possible supports into account, can still lead to significantly different results compared to studies on crystalline samples. In general, the above considerations suggest that low-coordinated cobalt atoms are more prone to the oxidation by water in a hydrogen environment and that the water partial pressure as well as the total hydrogen pressure play a significant role.

### 5.3.3 Metallic Co(0001) in CO

Figure 5.11 displays the change of the O 1s signal on Co(0001) while introducing CO into the near-ambient pressure cell at 220 °C surface temperature. The adsorbed oxygen on the as-prepared sample is efficiently removed as soon as the CO is introduced

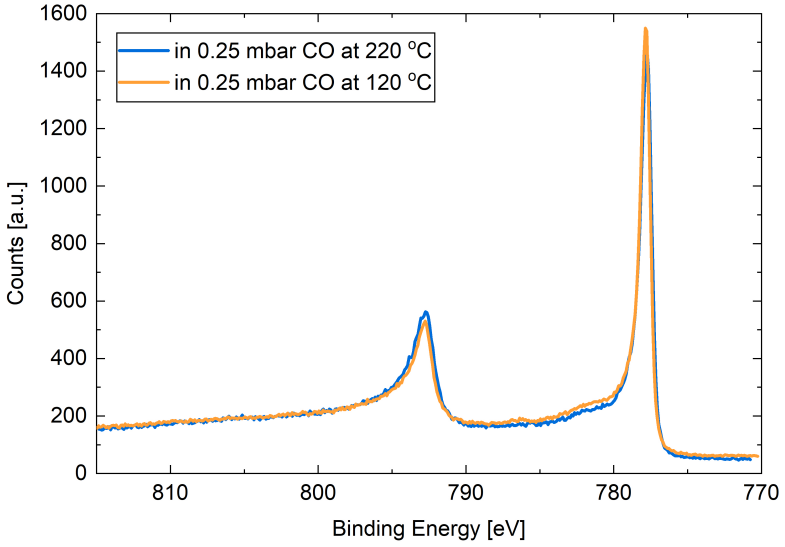


Figure 5.12: Co 2p areas measured on Co(0001) in 0.25 mbar CO at 220 °C and 120 °C.

(see horizontal reference line). At the same time the adsorbed CO signal appears at higher binding energy, albeit not yet to a strong extent compared to the adsorbed O on the as-prepared sample (see Section 5.3.5 for a quantitative analysis of the adsorbed species in 0.25 mbar CO).

The Co 2p signals displayed in Figure 5.12 confirm that the cobalt stays mainly metallic in 0.25 mbar CO at 220 °C (0.5 % oxidized contribution in the fit). This is is still the case when decreasing the temperature to 120 °C (4 % oxidized contribution in the fit). Thus, although the CO contains a similar amount of water (see Table 5.1) and is not additionally dried, it is significantly more efficient at keeping the Co(0001) metallic compared to dried $H_2$ at the same total pressure. This is especially surprising as the CO is expected to dissociate on defect sites starting from around 60 °C on [272]. Thus, at least part of the resulting adsorbed atomic oxygen (see Section 5.3.5) desorbs as $CO_2$ without oxidizing the cobalt.

These results are in agreement with the measurements of Wu et al. [226] on cobalt foil, which stays metallic even at room temperature in roughly 0.13 mbar CO. Additionally, they measure the reduction of CoO/Co(0001) by CO between 150 °C and 200 °C again indicating a kinetic limitation as well as the more efficient reduction by CO compared to $H_2$ at the same total pressure. $Co_3O_4$ powder has also been shown to start reducing in 0.15 mbar CO from 150 °C on, at lower temperatures than in 0.4 mbar $H_2$ [271]. In UHV studies, Kizilkaya et al. [229] observe the opposite behavior as $2 \cdot 10^{-5}$ mbar $H_2$ removes adsorbed oxygen from Co(0001) at 177 °C, whereas CO in the same pressure

range does not remove it even at 357 °C. In these conditions a coverage of at most 0.33 monolayers of CO and mainly on the top sites can be expected (estimated from Figure 8 in Ref. [245]). Based on the same reference, a coverage between 0.33 and 0.5 monolayers can be expected on the top as well as the hollow sites in all pressure and temperature conditions studied here (as well as industrial FTS conditions). As the top sites would be the most stable position for $H_2O$ as well [254,270], a specific minimal coverage with CO, thus minimal CO pressure at a specific temperature, could be needed for sufficient site blocking to prevent the oxidation. Combined TPD and DFT studies by Jiawei et al. [250] suggest that the adsorption of CO is significantly stronger than the adsorption of $H_2O$ such that the CO could adsorb preferentially when both are present in the gas phase. They also find that the co-adsorption of CO stabilizes the adsorption of $H_2O$ via hydrogen bonds. As molecularly adsorbed water can form two of those hydrogen bonds whereas OH could only form one, this might hinder dissociation of the adsorbed water.

As water preferentially adsorbs on the steps compared to on the Co(0001) terrace [269], the steps might be more relevant than the different terrace sites here. In contrast to $H_2$ (see Section 5.3.2), CO shows a comparable adsorption on stepped surfaces as on Co(0001) [273]. Thus, the blocking of step sites by the CO at the investigated pressures is possible. At the same time the dissociation of CO has been shown to be facilitated at the steps of Co(0001) compared to the terrace [272] and to not be hindered by an increasing CO coverage [274]. The dissociation could lead to additional blocking of the step edges by the resulting atomic carbon. As will be shown in Section 5.3.5, carbon species can be detected on the Co(0001) surface in CO at all investigated temperatures. Although the carbon atoms could diffuse on the terraces [266], they are more stable at the steps [218].

However, at even higher pressures, Groot et al. [242] observe the formation of CoO on Co(0001) in CO (purity 4.5 to 5) at temperatures up to 260 °C and no reduction up to 340 °C. In this case the total water pressure is higher such that the preferential adsorption of CO might be insufficient to block all sites for the $H_2O$ dissociation. However, in their study the total water pressure in both gases should be comparable and can thus likely not completely explain the significantly more efficient reduction they observe in $H_2$ compared to CO, which is in contrast to our results in the mbar range.

In general, the above suggested site blocking effect preventing oxidation could lead to a different result depending on the exact water content as well as the exact manner and order of introducing the CO and the oxidizing agent ($O_2$, $H_2O$, or wet $H_2$), which can further complicate the comparison of different studies in the literature.

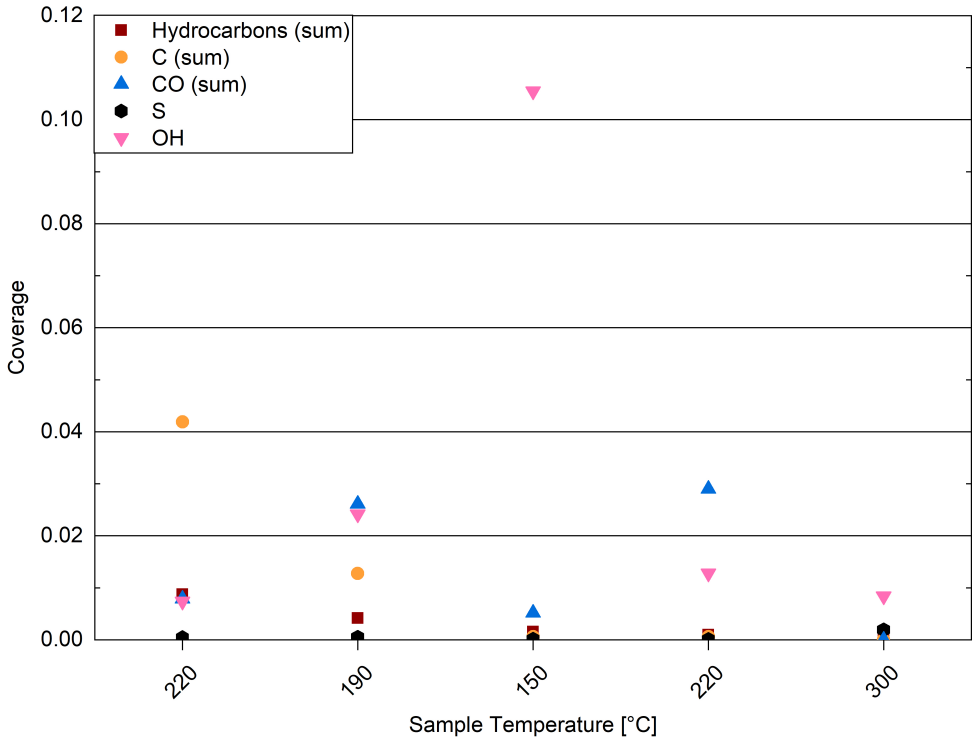


Figure 5.13: Coverages of adsorbed carbon species, OH, and sulfur on the Co(0001) surface in 0.25 mbar dried $H_2$ at different temperatures cooling down from 220 °C to 150 °C and subsequently heating up to 300 °C. For clarity the different carbon, hydrocarbon, and adsorbed CO peaks are summed up to one coverage each here and the detailed results are only displayed in the supplemental information. As explained in the text, the coverages can only be interpreted relatively to each other instead of absolutely in this case.

### 5.3.4 Adsorbed Species on Co(0001) in Hydrogen

Figure 5.13 displays the coverages of the adsorbed carbon species, OH, and sulfur on Co(0001) in 0.25 mbar dried $H_2$ at different temperatures. As explained in Section 5.2.3, the model to calculate these coverages does not take the oxidation of the surface (see Section 5.3.2) into account such that the resulting values can only be discussed as relative coverages with respect to each other here and are not absolute coverage values. As shown in Section 5.3.1, all as-prepared samples show some carbon. Here we start out with a carbon coverage of 0.04. It can clearly be seen that in time in $H_2$ the carbon is removed from the surface. This can be expected from around 150 °C surface temperature on [226]. Whereas the atomic C signal in the first measurement at 220 °C

consists of 23 % graphitic carbon and 77 % carbidic carbon, only carbidic carbon is left in all subsequent measurements (see Figure 5.21(a) in the supplemental information), suggesting that the graphitic carbon is removed first.
Interestingly, the hydrocarbons are removed as well while reducing the temperature from 220 °C to 150 °C (see Figure 5.13). As they can already be present on the as-prepared sample from the UHV background (see Section 5.3.1), the removal might not be related to the cooling but simply happen over time in $H_2$. On the other hand, hydrocarbons can stem from the hydrogen bottle. In this case it could be expected that more adsorb at lower temperatures. However, if that type of hydrocarbon needs to dissociate in a certain way to stick on the surface, they might only be present at higher temperatures. This is unlikely as they do not re-appear after heating to 300 °C. The two types of hydrocarbons differentiated in the fit do not show a clear trend (see Figure 5.21(b) in the supplemental information). In all investigated conditions the hydrocarbon signal is small with less than 0.01, which can lead to inaccuracies in such a detailed analysis.
The presence of some adsorbed CO is generally not surprising as there is a CO background in the UHV chamber as well as in the gas lines after previous uses of CO in the cell. However, no clear trend with temperature in $H_2$ can be recognized in Figure 5.13 except that no CO is adsorbed on the metallic Co(0001) at 300 °C. The difference between the other temperature steps, especially comparing the two different sets of measurements at 220 °C while cooling down and heating up again, could be explained on the basis of how much Co(0001) or CoO/Co(0001) is covered with other adsorbates (C, hydrocarbons, OH, and O) and how much is thus free for CO adsorption. The distinction between CO alone and CO co-adsorbed with O in the detailed fit (see Figure 5.21(c) in the supplemental information) shows that mainly the latter is present in those sets of measurements where the cobalt is oxidized. Thus, the binding energy of CO on CoO/Co(0001) is shifted as well and contributes to the peak that was identified as CO with co-adsorbed O. Therefore, it is not possible to use the position of the CO peak as an indication for the presence of adsorbed O on top of the CoO. However, the adsorbed OH, which also originates from dissociated water, is increased at these temperatures as well (see Figure 5.13). As the adsorbed oxygen contribution to the O 1s peak cannot be distinguished from the cobalt oxide, the presence of adsorbed oxygen on top of the oxide cannot be confirmed in a direct measurement. Whereas co-adsorbed oxygen would already reduce the probability for CO adsorption and CO dissociation [275], cobalt oxides favor CO oxidation over CO dissociation to such an extent that they are even investigated as CO oxidation catalysts [276].
Over the course of more than 7 h in 0.25 mbar $H_2$, a small amount of sulfur is adsorbed on the surface (0.002 in the last set of measurements at 300 °C), which likely stems

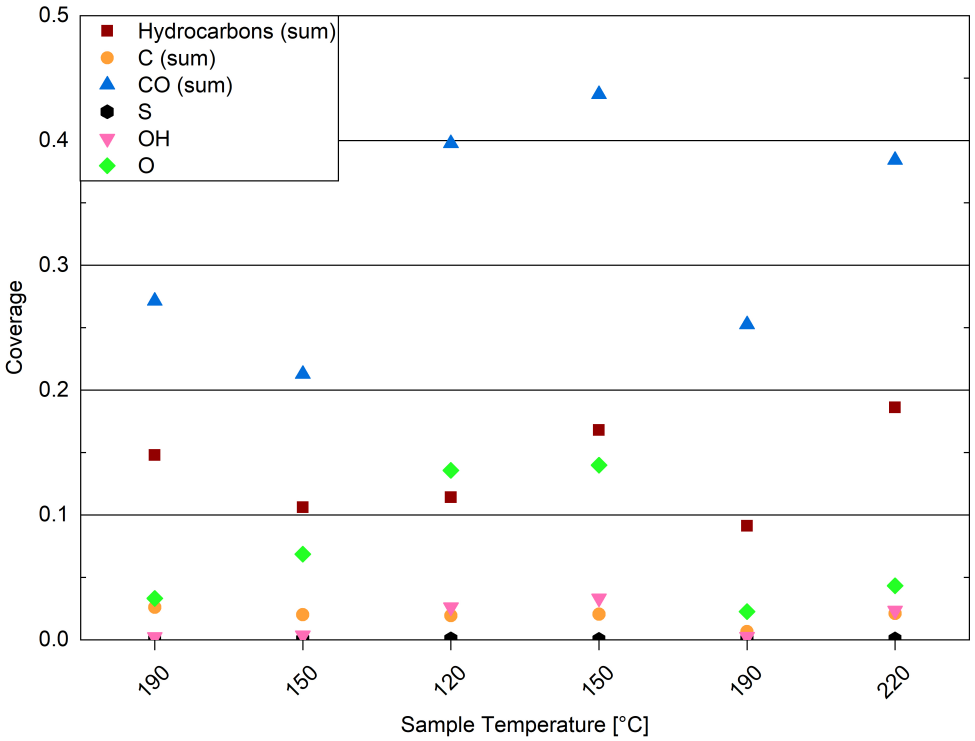


Figure 5.14: Coverages of adsorbed carbon species, oxygen species, and sulfur on the Co(0001) surface in 0.25 mbar CO at different temperatures cooling down from 190 °C to 120 °C and subsequently heating up to 220 °C. For clarity the different carbon, hydrocarbon, and adsorbed CO peaks are summed up to one coverage each here and are only displayed in detail in the supplemental information.

from contaminants in the hydrogen bottle.

### 5.3.5 Adsorbed Species on Co(0001) in CO

Figure 5.14 displays the calculated coverages of the adsorbed species on Co(0001) in 0.25 mbar CO at different temperatures. With a maximum coverage below 0.15, less oxygen than on the as-prepared sample in UHV is present. This confirms the removal of adsorbed oxygen by CO described in Section 5.3.3. Still, a trend to increasing oxygen coverage with decreasing temperature is observed. Adsorbed OH, although significantly less than O (as in UHV as well as in $H_2$), follows the same trend confirming that again both likely stem from dissociation of background water. Additionally, this confirms that O from CO dissociation at defect sites is mostly removed as $CO_2$ as expected

from literature [226,245].
The range of CO coverages measured (between 0.21 and 0.44) is slightly lower than the expected range between 0.33 to 0.5 monolayers (see Figure 8 in Ref. [245]). However, taking into account how much surface area is in total occupied by other species, the CO coverage on the bare part of the surface area can be calculated as between 0.27 and 0.68. This estimate does not take possible interactions between the different adsorbates as well as changes over time (see below) into account.
The CO coverage shown in Figure 5.14, which is calculated based on the C 1s spectra, is not generally higher at lower temperatures. Figure 5.22(a) in the supplemental information compares these CO coverages to the CO coverages calculated from the O 1s spectra. Whereas the latter is generally higher at lower temperatures, the C 1s spectrum shows more adsorbed CO in the first measurement at 190 °C as well as after heating up to 220 °C again. As the C 1s spectra are measured right after changing the temperature and the O 1s spectra roughly 18 min later, this could be related to a carbon and/or hydrocarbon built-up over time, which is especially expected at the temperatures active for FTS (as well as beam-induced reaction, see Section 5.5.1). Thus, although no change in the carbon signal can be detected on the time scale of the C 1s measurement, it could be detected indirectly as less surface area is free for CO, OH, and O adsorption once the O 1s spectrum is measured.
The CO in the O 1s spectrum, the CO in the C 1s spectrum, as well as the adsorbed O and OH show a (slightly) higher coverage after heating to 150 °C compared to their coverage at 120 °C. As this trend is the same in the C 1s and the O 1s spectrum, it cannot be caused by the time difference between the two measurements (as the effect explained in the previous paragraph). However, an increase in any adsorbate towards the end of a set of measurements can cause an inaccuracy in all coverages at once as the Co 2p signal (which is measured at the end of the set) is then underestimated. All calculated coverages, which are roughly inverse proportional to the measured Co 2p intensity (see Equation 5.7 in Section 5.2.3), are thus overestimated at the same time. Taken the estimated inaccuracy of $\pm$ 0.05 for all coverages into account, the CO and O coverages at 120 °C and subsequent increase to 150 °C are overall comparable. Comparing the coverages at 150 °C before and after the cooling to 120 °C, a hysteresis between adsorption and desorption can thus be observed.
As explained in Section 5.2.2, two peaks are associated with adsorbed CO (without co-adsorbed O) in the C 1s signal, a main higher binding-energy peak as well as a lower binding-energy peak that was tentatively identified as a second, less stable adsorption site on the Co(0001) terrace. At all temperatures investigated here, most of the CO (without co-adsorbed O) is located at the most stable site (between 83 % and 88 %) confirming this identification. Compared to the phase diagram for CO adsorption by

Weststrate et al. (Figure 8 in Ref. [245]), it is likely that the most stable site is the top site, whereas the second observed one is the hollow site. As the coverage of CO (without co-adsorbed O) does not change significantly with the different temperatures investigated here (see Figure 5.22(b) in the supplemental information), a constant ratio of the two different adsorption sites is not surprising. Instead the change in CO adsorption with temperature is detected mainly in the peak identified as CO with co-adsorbed O (agreeing with the change in adsorbed O). This CO with co-adsorbed O consists of two peaks in the detailed C 1s fit as well. Here, the lower binding energy one is dominant (thus likely the most stable site) and accounts for between 71 % and 83 % of the CO co-adsorbed with O. Thus, although the total CO coverage varies in a range from 0.21 to 0.44 depending on the temperature (see Figure 5.14), the distribution over the different adsorption sites remains comparable for CO both with and without co-adsorbed O.

The change of the amount of adsorbed hydrocarbons with temperature appears somewhat correlated to the amount of adsorbed CO. If all hydrocarbons stemmed from the CO bottle, one could expect that the adsorbed amount is simply correlated to the temperature like the adsorbed O or to the free space on the surface, which can be estimated from the total amount of all other adsorbates. In this case more adsorbed hydrocarbons could be expected after decreasing the temperature to 150 °C. On the other hand, a larger hydrocarbon coverage at higher temperatures from 190 °C on could be expected if the hydrocarbons are formed through reaction of the adsorbed CO with background hydrogen. The distinction between two different hydrocarbon peaks in the detailed fit (see Figure 5.22(c)) shows that one type is increased at higher temperatures (type I) and might thus be the hydrocarbons that are produced by reaction with background $H_2$, whereas the other type (type II) is adsorbed more at lower temperatures and could stem from the background in the CO bottle.

The absolute atomic carbon coverage is not significant with values between 0.007 and 0.021, such that the change with temperature is within the estimated inaccuracy of the calculated coverages. Although CO dissociation, which can be expected from 60 °C on [272], could leave carbon behind, the amount of carbon is in the same range as on the as-prepared sample in UHV (see Section 5.3.1). Thus, it cannot be related to CO dissociation unambiguously. However, in contrast to the UHV measurements, the detailed fit (see Figure 5.22(d) in the supplemental information) suggests that the carbon is mainly present as graphitic carbon, whereas a smaller amount of carbidic carbon that appears when decreasing the temperature to 150 °C is not visible anymore after increasing it to 190 °C again. The carbidic carbon can diffuse into the bulk, although we have observed that only from higher temperatures on in UHV (see Section 5.3.1). It is more likely that carbon is removed by reaction with background $H_2$ from 190 °C

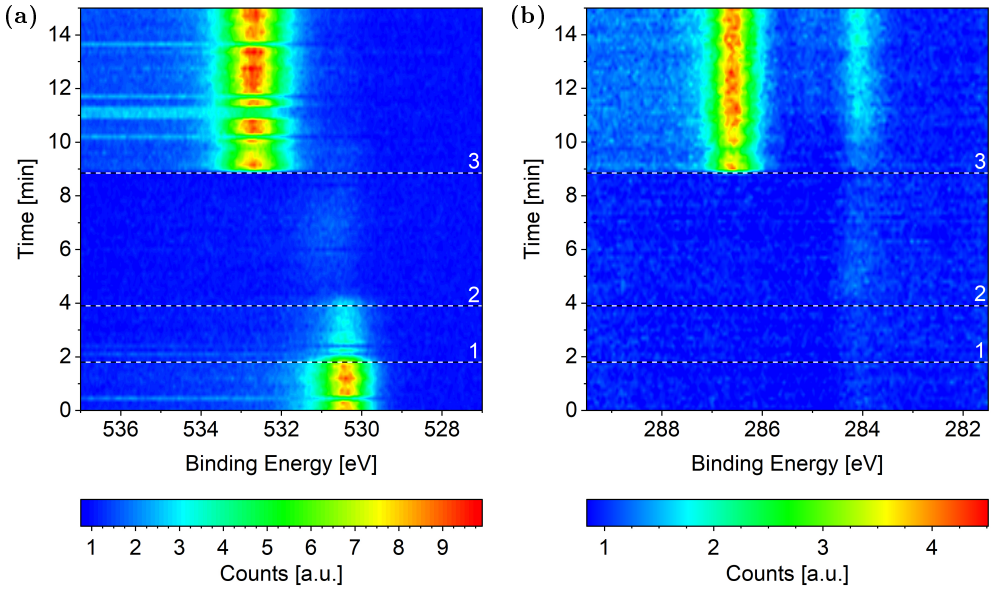


Figure 5.15: Change of the (a) O 1s and (b) C 1s signals measured on Co(0001) over time while introducing the reaction mixture of 4 $H_2$ + 1 CO at 220 °C. The three black and white reference lines mark (1) the moment the mass flow controllers are connected to the cell, (2) the start of the flow of 4.4 ml/min $H_2$, (3) and the start of the flow of 1.1 ml/min CO. All consecutive spectra have been normalized to the background level at low binding energy. Some faulty measurements caused by an insufficient delay between the different scans are visible as horizontal lines in (a).

on (see Section 5.3.4). Interestingly, the graphitic carbon seems to be present in larger amounts at higher temperatures. This could be due to a higher rate of CO dissociation or also be related to the decrease in carbidic carbon at those temperatures. If some carbidic carbon would become graphitic, it might not lead to a net change in the total carbon coverage. The graphitic carbon could then be more resistant to removal by the low background pressures of $H_2$ (details see following section).
The sulfur coverage detected after a total of more than 17 h in 0.25 mbar CO is less than 0.001.

### 5.3.6 Adsorbed Species on Metallic Co(0001) during FTS

Starting from the as-prepared Co(0001) in UHV the reaction mixture was introduced by first starting the flow of dried $H_2$ and, once all adsorbed oxygen has been removed, starting the additional flow of CO. This can be seen in Figure 5.15(a) in the form of the removal of O and the subsequent adsorption of CO at higher binding energy.

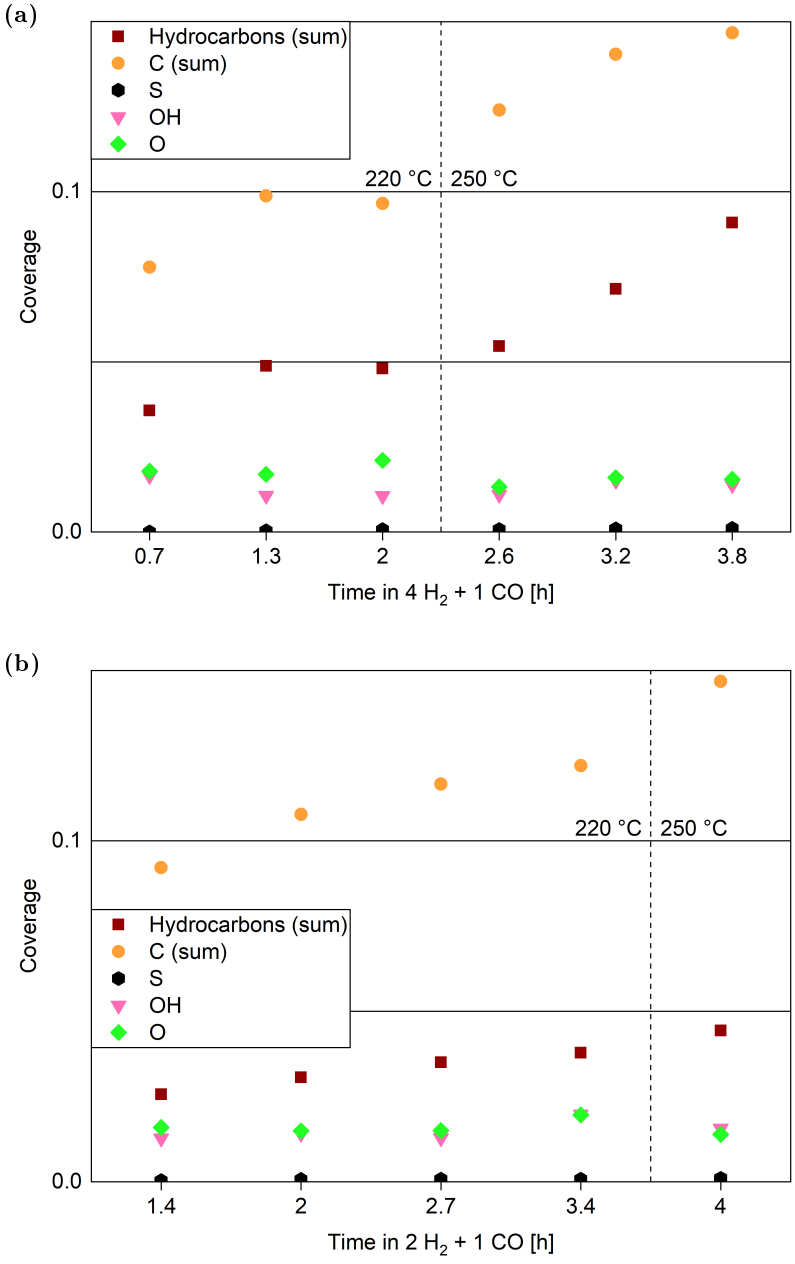


Figure 5.16: Coverages of carbon species, oxygen species, and sulfur on Co(0001) in 0.25 mbar (a) 4 $H_2$ + 1 CO and (b) 2 $H_2$ + 1 CO. The temperature is increased from 220 °C to 250 °C at the dotted, vertical reference line. For clarity the different atomic carbon and hydrocarbon peaks are summed up to one coverage each here and are only displayed in detail in the supplemental information.

The removal of oxygen seems to start already before setting the hydrogen flow. At reference line 1 the mass flow controllers are connected to the cell by opening certain valves. This can easily cause a partial reduction by background gas from the lines or small amounts of $H_2$ or CO leaking through the mass flow controllers. Right after the start of the CO flow the adsorbed CO as well as carbon and some hydrocarbons can be seen in the change of the C 1s signal in Figure 5.15(b). Additionally, a small amount of adsorbed OH and some carbon or hydrocarbon species could be suspected in $H_2$ (between reference line 2 and reference line 3). However, these are not significant compared to the background level.

As the cobalt stayed metallic in 0.25 mbar dried $H_2$ (see Section 5.3.2) as well as 0.25 mbar CO (see Section 5.3.3) at 220 °C, it could be expected that it also stays metallic in a mixture of the two gases at the same total pressure and temperature. This is confirmed by an oxidized contribution to the Co 2p fit of at most 3 % during up to 3 h in a 4:1- or a 2:1-ratio of $H_2$ to CO at 220 °C. At 250 °C the same value is measured. Thus, the additional water produced in the Fischer-Tropsch reaction is not sufficient to oxidize the surface under these conditions.

Figure 5.16 displays the coverages of the adsorbed species on Co(0001) at the two different gas ratios. In line with the removal of oxygen described above, the O coverage stays between 0.015 and 0.02 for both gas ratios at 220 °C, and is only slightly lower with a maximum of 0.016 at 250 °C. The OH coverage is comparable with values between 0.01 and 0.02. These values are on the same order of magnitude as on the metallic surface in 0.25 mbar CO at 220 °C. As shown in Section 5.3.5, the O coverage can still be an order of magnitude higher upon decreasing the temperature while the surface stays metallic. In UHV the O coverage is even higher with $0.25 \pm 0.05$ without oxidizing the surface (see Section 5.3.1). However, in 0.25 mbar dried $H_2$ the surface did oxidize at lower temperatures (see Section 5.3.2). In the two reaction mixtures lower temperatures were not investigated here. However, the observation that the surface is metallic at 220 °C is in rough agreement with the reduction of oxidized cobalt foil seen from 225 °C on in 0.1 mbar 1 $H_2$ + 1 CO [226], as well as the reduction of CoO/Co(0001) observed in 1 bar 1 $H_2$ + 1 CO above 220 °C [242]. As mentioned above, the complexity of catalysts, supports, and promoters can strongly influence the oxidation and catalytic behavior. This is evidenced by observations of positive as well as negative effects of water on the activity and selectivity of different cobalt-based catalysts [277–279]. Overall, the poisoning by oxidation is believed to not play a large role for industrial Fischer-Tropsch synthesis as it can easily be prevented under realistic conditions [222].

Figure 5.17 displays the CO coverage in the reaction mixture (compared to the other adsorbed species). The absolute value of CO coverage lying between 0.44 and 0.53

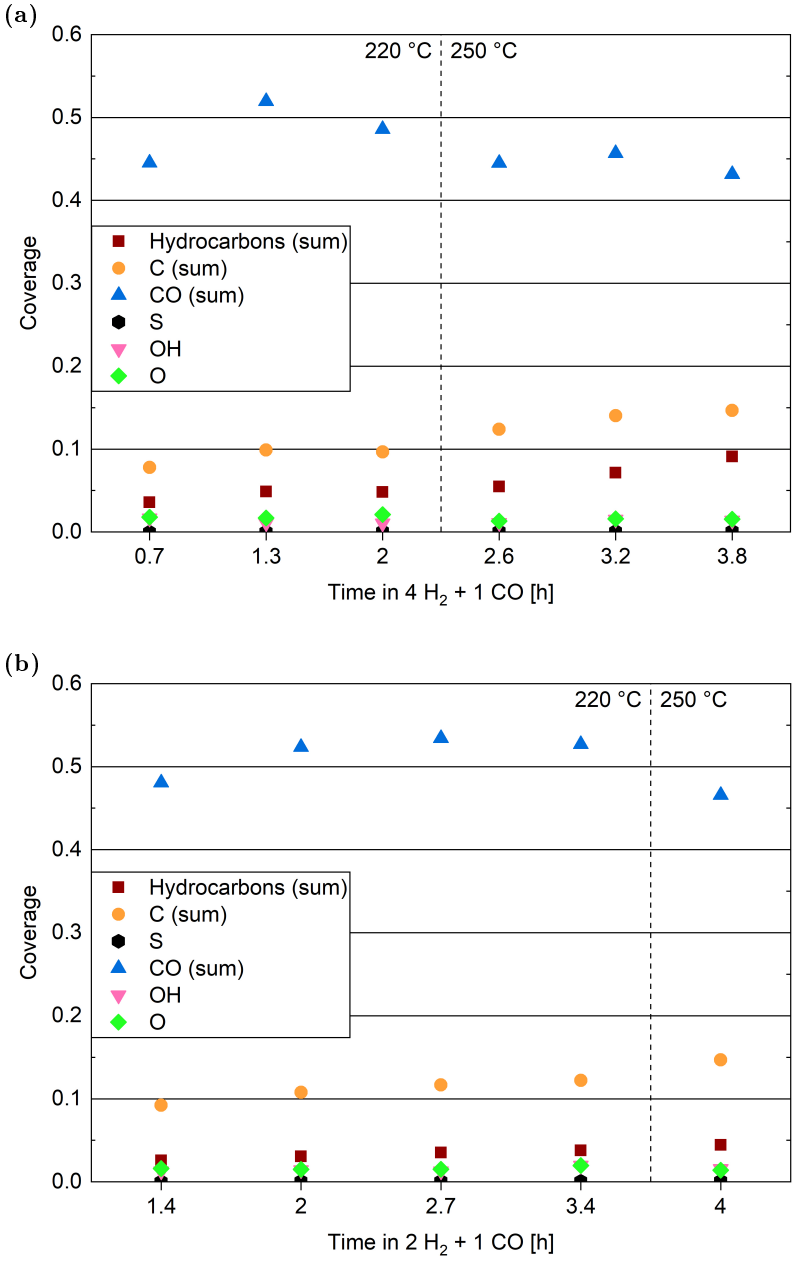


Figure 5.17: Coverage of CO on Co(0001) in 0.25 mbar (a) 4 $H_2$ + 1 CO and (b) 2 $H_2$ + 1 CO. The temperature is increased from 220 °C to 250 °C at the dotted, vertical reference line. For clarity the sum of the different CO peaks is shown here and the results are only displayed in detail in the supplemental information. For comparison the coverages of all other adsorbed species from Figure 5.16 are plotted again.

seems somewhat higher in reaction conditions compared to 0.25 mbar CO at 220 °C (see Figure 5.14 in Section 5.3.5). However, less other species are adsorbed here. The coverage on the bare part of the surface is comparable for both gas mixtures and lies between 0.52 and 0.63 at 220 °C. Thus, this is not significantly different from the value of 0.53 measured in 0.25 mbar CO at 220 °C. A trend to smaller absolute CO coverages in the reaction mixtures at 250 °C compared to 220 °C is not significant and can be explained by the increase of other carbon species. The CO coverage on the bare part of the surface is calculated to be between 0.59 and 0.60 at 250 °C and is thus in the same range as at 220 °C. These results are roughly in agreement with the expected CO coverage of 0.5 during the reaction [245] and confirm that it does not strongly depend on the CO partial pressure or the temperature under the conditions investigated here. As only a small amount of adsorbed O is detected in reaction conditions, it is not surprising that the adsorbed CO is mainly found in the peaks associated with CO without co-adsorbed O (see Figure 5.23(a) in the supplemental information). The two different peaks associated with adsorbed CO without co-adsorbed O further show that between 93 % and 97 % of the CO is adsorbed in the most stable site, which is likely the top site. Thus, although the absolute coverage in reaction conditions is comparable to in CO (see Section 5.3.5), a somewhat higher fraction of it is in the top site. This might be related to the smaller amount of other adsorbates, which allows more CO to sit in the preferred position.

The atomic carbon coverage during the reaction is displayed in Figure 5.16. Although an increasing trend is visible at 220 °C, the C coverage stays between 0.08 and 0.12 over a time of 3 h at this temperature. In the first measurement in time the C coverage is already significantly more than in $H_2$ or CO at 220 °C suggesting that it is caused by the Fischer-Tropsch reaction. Taking the different time axes in Figure 5.16(a) and Figure 5.16(b) into account, the carbon deposition is not faster in 2 $H_2$ + 1 CO than in 4 $H_2$ + 1 CO suggesting that the removal of C is not limited by the exact $H_2$ partial pressure in this pressure range. Although there seems to be a jump in the C coverage when increasing the temperature to 250 °C, the further C deposition at this temperature (measured only in 4 $H_2$ + 1 CO) does not clearly display a larger rate than at 220 °C. Thus, any increase in the rate of CO dissociation with increased temperature seems to be compensated by a faster C removal by $H_2$. These observations seem to be in contrast to magnetometer studies on an industrial catalyst where the rate of carbide formation, although deemed insignificant in general, was found to decrease with an increased $H_2$-to-CO-ratio as well as with increased temperature [280]. However, a direct comparison of such literature to our experiments is not justified given the use of a single crystal, the lower pressure range, and significantly shorter time frame investigated here. It is especially unclear whether the C deposition would keep increasing linearly over

time, thus covering the whole surface after on the order of tens of hours, or whether it would saturate at a certain coverage in an equilibrium between deposition and removal. Generally, only specific polymeric, graphitic, and bulk carbides are deemed a poison to the catalyst [216,219,246], whereas all surface carbon that is hydrogenated at FT gas ratios and temperatures can be considered a reaction intermediate. Figure 5.23(b) in the supplemental information shows that, although both carbidic and graphitic carbon follow a similar trend in time, most adsorbed C is carbidic. However, our results in Section 5.3.4 show that both forms of carbon detected here could be removed by exposure to 0.25 mbar $H_2$ and are thus likely not carbon species responsible for significant catalyst poisoning.

Starting out with an absolute value of 0.04 and 0.03 at 220 °C respectively, in both reaction mixtures there are more hydrocarbons adsorbed than in UHV and $H_2$, but they are in the same order of magnitude as in 0.25 mbar CO (see Section 5.3.5). However, the absolute hydrocarbon coverage is higher in 4 $H_2$ + 1 CO than in 2 $H_2$ + 1 CO, thus scaling inversely with the CO partial pressure. This can for example be seen by comparing the measurement after 2 h at 220 °C and the first measurement at 250 °C for the two different gas ratios in Figure 5.16. Thus, it can be excluded that all hydrocarbons stem from the background of the CO gas. Additionally, the hydrocarbon coverages follow roughly the same trend over time as the C coverage including a stronger increase after increasing the temperature indicating that at least part of the hydrocarbons could stem from the same reaction process as the carbon. Under industrial conditions on cobalt catalysts a higher $H_2$-to-CO-ratio has a positive effect on the turnover for short products and switches to a negative effect on the turnover for longer products from a length of roughly 15 carbon atoms on [281]. This can be explained by a decreased chain growth probability $\alpha$ in the Anderson-Schulz-Flory chain-growth model [282] with increasing $H_2$-to-CO-ratio. On Co(0001), the Fischer-Tropsch product distribution decreases exponentially from methane to longer chains with mainly $C_1$ to $C_4$ products detected at atmospheric pressures [243,283]. Therefore, mainly methanation is measured on Co(0001) in the mbar range [127]. The methane turnover on Co(0001) does increase with increasing $H_2$-to-CO-ratio [284,285]. Thus, mainly shorter products can be assumed here and a higher activity in 4 $H_2$ + 1 CO compared to 2 $H_2$ + 1 CO is likely. However, even if it is the main product, methane will likely not stay adsorbed on the Co(0001) surface [286] and is thus likely not the species detected by XPS. In contrast, it can be expected that the adsorption strength of the products increases roughly linearly with the chain length [287,288], which results in an exponential increase in the residence time on the surface. Based on this assumption Navarro et al. [47] have modeled the adsorption of products on Co(0001) over time. Their result that a chain length of at least 15 carbon atoms is needed to

reach a significant coverage on the surface agrees well with the length they find experimentally. As our experiments are done at lower pressures, it is to be expected that a full coverage with products could only be reached after a significantly longer time than the 30 min Navarro et al. [47] observed in the same temperature range. The sum of the coverages of all adsorbates stays within 0.6 to 0.7 for both reaction mixtures over the time of hours tested here. This confirms that the surface is not fully covered with products and excludes any influence of space limitation on the measured coverages. To shed more light on the nature of the adsorbed hydrocarbons, Figure 5.23(c) in the supplemental information distinguishes the two different peaks contributing to the overall hydrocarbon coverages displayed in Figure 5.16. In both gas ratios the two types show a similar increase over time at 220 °C with the hydrocarbon type labeled II clearly being dominant (at least 70 % of the total hydrocarbon coverage). However, at 250 °C the amount of type I strongly increases over time, whereas type II starts to desorb. If both hydrocarbons were from the reaction, one would have to conclude that the increase of the desorption rate of type II strongly exceeds the increase of the rate of its formation when increasing the temperature from 220 °C to 250 °C, whereas for type I the increase of rate of formation strongly exceeds the increase of the desorption rate when increasing the temperature from 220 °C to 250 °C. As type I is more strongly adsorbed, it would be a longer hydrocarbon than type II in this case. However, the formation of different products shows a comparable temperature dependence on Co(0001) [283], whereas in industrial FTS the product distribution would rather shift to shorter chain lengths with increasing temperature [212]. Therefore, we deem it more likely that the hydrocarbon type II stems from the gas background whereas type I is a reaction product, which agrees with the results of Section 5.3.5. Generally, the deposition of products, although it can poison the catalyst [216], can also be considered part of the initiation phase of the catalyst after which the desorption of subsequent products is facilitated [47].
The sulfur coverage increases to maximally 0.001 within 4 h in the reaction mixture for both gas ratios. Thus, although sulfur is known to easily block CO oxidation on Co(0001) [220,289] as well as more industrially relevant catalysts [221], it is not a significant poison in the conditions and time frame studied here.

## 5.4 Conclusions and Outlook

Generally, the oxidation behavior of cobalt during FTS depends on a number of factors: the structure of the sample, the water partial pressure, and the $H_2$-to-CO-ratio. For the case of Co(0001), CO is more efficient at keeping the cobalt metallic compared to $H_2$ at the same total pressure of 0.25 mbar as measured here by in situ XPS. We have

suggested that this behavior can be explained on the basis of the different adsorption and dissociation sites of $H_2$, CO, and $H_2O$, respectively. Namely, CO adsorbs equally well on the steps and vacancies as on the terrace sites and is therefore able to block the dissociation of water, which most likely proceeds at low-coordinated sites. In comparison, $H_2$ prefers the Co(0001) terrace sites for adsorption and can therefore not prevent the $H_2O$ dissociation in this pressure range. Under reaction conditions of 4 $H_2$ + 1 CO and 2 $H_2$ + 1 CO at 220 °C to 250 °C the surface stays mainly metallic.
We have developed a theoretical model to convert the measured intensities of all adsorbed species to quantitative coverage values. Comparisons to values expected from literature have confirmed the validity of this model in combination with an experimental calibration.
The high-resolution carbon areas measured at the HIPPIE beamline of MaxIV allow for the distinction of a number of species. In this way it can be seen that at least 70 % of the carbon adsorbed on the surface during the reaction at 220 °C is carbidic and thus a reaction intermediate that can easily be removed by hydrogenation. Additionally, two different hydrocarbon peaks in the fit allowed for the distinction of hydrocarbons adsorbed from the CO gas background and formed by the Fischer-Tropsch reaction.
We plan to further study the effect of the water partial pressure on the oxidation behavior of Co(0001) by recording phase diagrams with and without drying of the gases. At a high-flux beamline this can be done via quick O 1s, C 1s, and Co 2p scans while continuously changing the conditions within a larger range of $H_2$-to-CO-ratios and temperatures. Additionally, the identification of the different CO adsorption peaks should be confirmed by more detailed studies in a larger CO pressure range from UHV to mbars.

## 5.5 Supplemental Information

### 5.5.1 Beam-induced Deposition

Figure 5.18 compares the carbon and hydrocarbon coverage measured over time in the reaction mixture at 220 °C while staying in one position on the surface (thus with strong beam exposure) to measurements where the beam exposure was minimized. To achieve the minimum beam exposure we have moved to a new position on the sample right before every measurement of the carbon area. In this way the influence by the beam is as small as possible and stays constant over time between measurements taken at the same temperature. When comparing two consecutive sweeps of every such carbon area measurement, no difference is detectable, which confirms that the beam-induced deposition does not play a role in the time frame in which the carbon signal is measured. However, as the O 1s and Co 2p areas are measured later in time, they

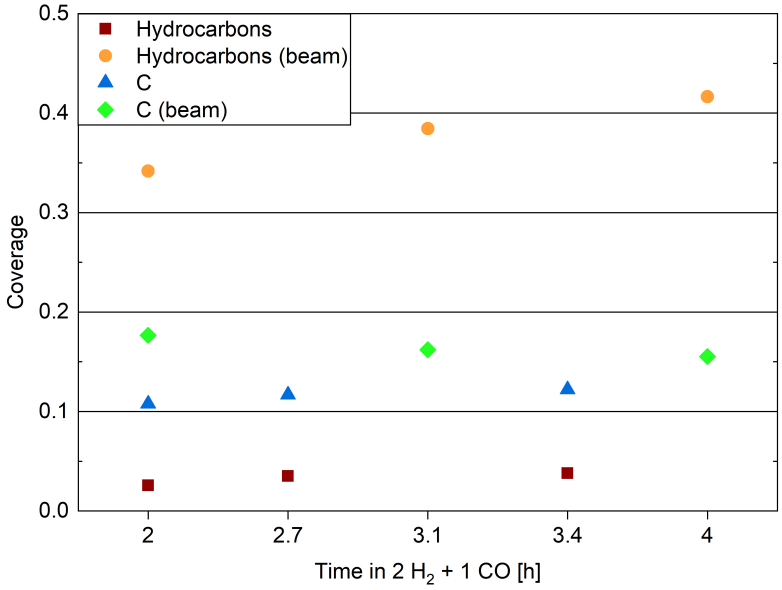


Figure 5.18: Coverages of carbon and hydrocarbons measured on Co(0001) in 0.25 mbar 2 $H_2$ + 1 CO at 220 °C over time comparing measurements done with strong beam exposure, labeled (beam), to measurements done while minimizing beam exposure as explained in the text.

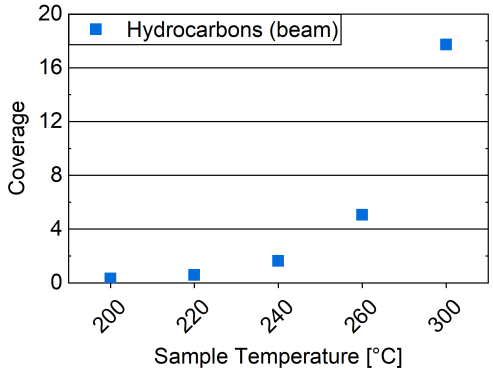


Figure 5.19: Hydrocarbon coverage on Co(0001) measured in 0.25 mbar 2 $H_2$ + 1 CO at increasing temperature. The sample was held at every temperature step for roughly 2.5 h under continuous beam exposure at the same position. As explained in Section 5.2.3, the coverage values displayed here are calculated as the number of layers that would be present if the hydrocarbons covered the whole surface in the absence of other adsorbates.

could still be slightly influenced by a change in carbon species over time. The same procedure is used for all measurements shown in the previous sections.
In detail, the comparison in Figure 5.18 shows a somewhat higher coverage of C, likely stemming from beam-induced CO dissociation. Subtracting the two values at 2 h results in a maximum beam-induced C coverage of 0.07. However, this difference decreases over time, likely because more surface area gets blocked by hydrocarbons on the surface with strong beam exposure. The detailed fits show that between 69 % and 80 % of the carbon is carbidic on the beam-exposed sample. This is in the same range as on the sample with minimized beam exposure (70 % to 76 %), thus not suggesting any promotion of graphite formation by the beam.
The deposition of hydrocarbons is more strongly increased on the sample with strong beam exposure, roughly by a factor of 10 compared to the sample with minimum exposure. This suggests a beam-induced Fischer-Tropsch reaction. The detailed fits show that all of the beam-induced hydrocarbon is the one labeled here as type I. This is the type identified as a Fischer-Tropsch product of the cobalt-catalyzed reaction in Section 5.3.6. There, it was formed significantly faster at 250 °C compared to at 220 °C. Thus, the beam might practically have a similar effect as an increased temperature. The beam-induced deposition could be observed starting from 220 °C surface temperature on and proceeds faster at higher temperatures. While increasing the temperature from 220 °C to 300 °C in the reaction mixture over a course of roughly 8 h, the hydrocarbon coverage increased exponentially (see Figure 5.19) and reached a total of 18 layers. As explained in Section 5.2.3, at these kind of coverages the model used for the calculations is not accurate and this is thus a rough estimate at best. However, it is clear that the cobalt terraces are completely covered before reaching this amount of hydrocarbons. This additionally suggests that the cobalt surface itself might not be necessary for the beam-induced reaction, although the steps could still be involved. In contrast to type II, the hydrocarbon type I does not seem to desorb in the temperature range investigated here, thus being able to cover the whole surface and making it crucial to minimize the beam exposure.

### 5.5.2 Detailed Fit Results

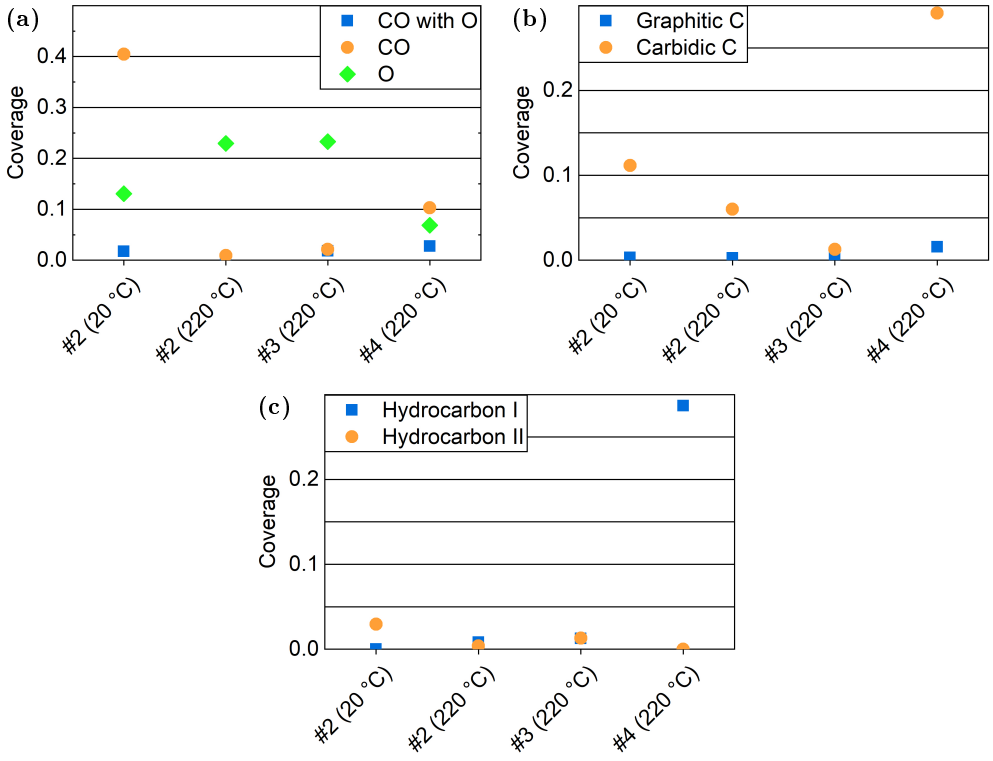


Figure 5.20: Results of the detailed fits of C 1s spectra measured on different as-prepared samples in UHV (a) distinguishing CO alone from CO co-adsorbed with O compared to the O coverage from the O 1s spectra, (b) distinguishing carbidic and graphitic C, and (c) distinguishing two types of hydrocarbons.

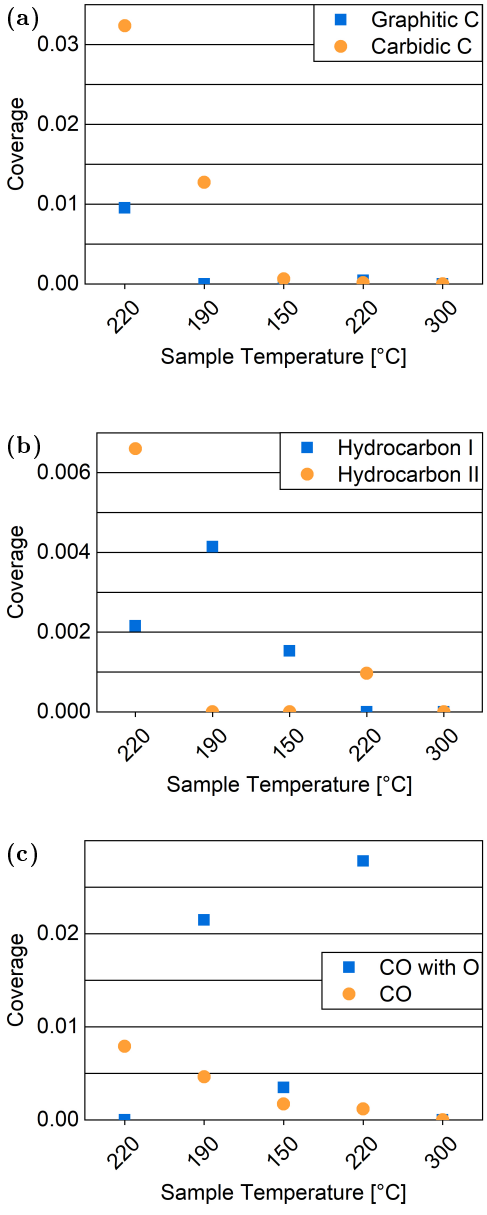


Figure 5.21: Results of the detailed fits of C 1s spectra measured in 0.25 mbar $H_2$ at different temperatures distinguishing (a) carbidic from graphitic C, (b) two types of hydrocarbons, and (c) CO alone from CO co-adsorbed with O.

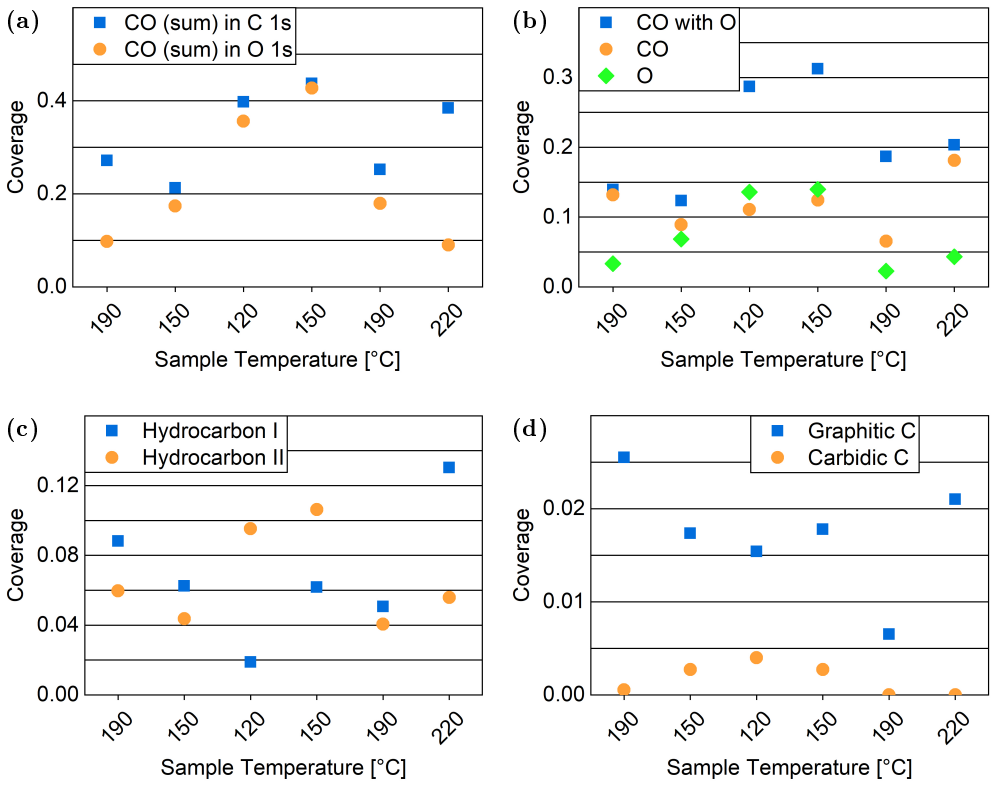


Figure 5.22: Results of the detailed fits of the spectra measured in 0.25 mbar CO at different temperatures (a) comparing the total CO coverage calculated from the C 1s spectra to the total CO coverage calculated from the O 1s spectra, (b) distinguishing CO alone from CO co-adsorbed with O compared to the O coverage, (c) distinguishing two types of hydrocarbons, and (d) distinguishing carbidic from graphitic C.

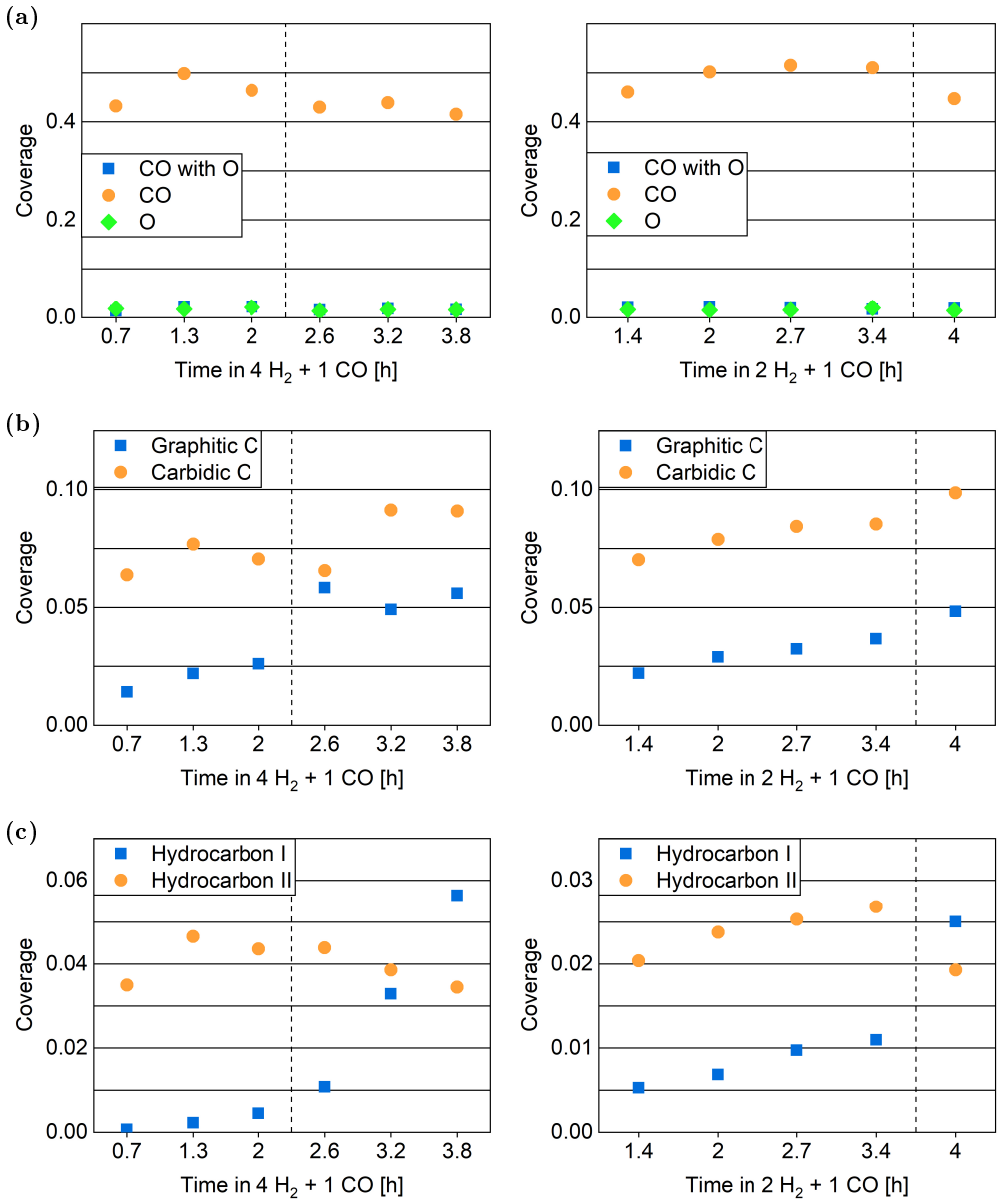


Figure 5.23: Results of the detailed fits of C 1s spectra measured in 0.25 mbar of 4 $H_2$ + 1 CO (left column) and 2 $H_2$ + 1 CO (right column) (a) distinguishing CO alone from CO co-adsorbed with O compared to the O coverage from the O 1s spectra, (b) distinguishing carbidic from graphitic C, and (c) distinguishing two types of hydrocarbons. The dashed, vertical lines mark an increase of the temperature from 220 °C to 250 °C.